NAG-1801

Design and Analysis for CubeSat Missions

A Major Qualifying Project Report

Submitted to the Faculty of the
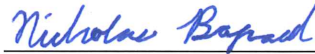
WORCESTER POLYTECHNIC INSTITUTE
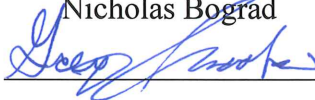
in Partial Fulfillment of the Requirements for the

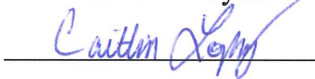Degree of Bachelor of Science

in Aerospace Engineering

by

Nicholas Bograd

Nicholas Bograd

Gregory Jacobson

Gregory Jacobson

Patrick Kroyak

Patrick Kroyak
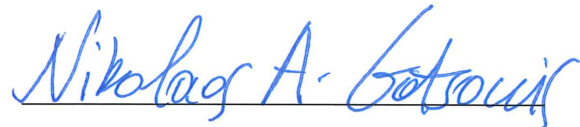
Caitlin Lopez

Caitlin Lopez

Jackson Peters

Jackson Peters

March 14, 2018

Approved by: *Nikolaos A. Gatsonis*

Professor Nikolaos A. Gatsonis, Advisor

Aerospace Engineering Program

WPI

Abstract

This project presents the mechanical design and orbital, thermal and magnetic interference analysis for two Cube Satellites (CubeSats) that feature onboard propulsion. The four-unit (4U) CubeSat is designed for flight at altitudes below 250 km. The 16U CubeSat is designed to raise its orbit to altitudes above 500 km. SolidWorks is used for the mechanical design of the CubeSats including all subsystems. Orbital decay analysis with Systems Tool Kit shows that both CubeSats have compliant lifetimes. Thermal analysis with COMSOL using de-featured design models of the CubeSats and unsteady heat loads expected during the orbits, shows that component temperatures are close to tolerances. COMSOL is used for a preliminary assessment of potential magnetic interference by candidate magnetic torquers.

Acknowledgements

We would like to thank the following people for their continued help with this project, without whom its completion would not have been possible.

Project Advisor:	Professor Nikolaos Gatsonis
ADC Team:	Professor Michael Demetriou and the (MAD-1801) Team
PTCC&DH Team:	Professor John Blandino and the (JB-1801) Team

Authorship

Introduction	
1.1, 1.2, 1.3	NB, GJ, PK, CL, JP
1.4.1	NB, PK
1.4.2	GJ, CL, JP
Mechanical Design	
2.1	NB
2.1.1	JP
2.2	NB, PK
2.3	NB, PK
2.4,2.4.1	GJ, JP, CL
2.5	GJ, CL
2.6	GJ
Orbital Lifetime Analysis	
3	JP, PK
Thermal Analysis	
4.1	NB
4.1.1,4.1.2	NB
4.2	JP
Magnetic Interference Analysis	
5.1	PK
5.2	PK
5.3	CL
Conclusion and Recommendations	
6.1	NB, PK
6.2	JP

Contents

Figures

Tables

1 Introduction

NASA defines small satellites as spacecraft weighing less than 180 kilograms (Mabrouk, 2017). Within the realm of small satellites NASA makes further subdivisions based on weight. These include: minisatellites (100-180 kg), microsatellites (10-100 kg), nanosatellites (1-10 kg), picosatellites (0.01-1 kg), and femtosatellites (0.001-0.01 kg). Cube satellites (CubeSats) are nanosats which are increasing in popularity due to their low complexity on board systems and low cost to build and operate. CubeSats come in a variety of sizes with the standard size unit (U) being a cube with dimensions of 10cm x 10cm x 10cm and an approximate mass of 1kg (Mabrouk, 2017). Common configurations for CubeSat missions include 1U, 2U, 3U and 6U, and are made by stacking the units. CubeSats are prized for their capability to be used for a variety of small scale missions, such as Earth observation, or to demonstrate new technological capabilities for future missions. The CubeSat program originated from a collaborative effort between Stanford University and California Polytechnic Institute (Cal Poly) in the fall of 1999. Under the leadership of Robert J. Twiggs, the program was intended to offer an educational opportunity for students to partake in a meaningful satellite mission that could be completed in 1 to 2 years (eoPortal Directory, 2018).

This MQP is a part of a larger Systems Engineering Group (SEG) which performs the conceptual design for two CubeSat missions. The first is a 4U CubeSat shown in Figure 1 slated to perform at extreme Low Earth Orbits down to 200 km. The CubeSat carries a propulsion system and the concept has been proposed by Blandino et al. (2016) and this project performs the design of the CubeSat. The second is a non-conventional 16 U CubeSat also shown in Figure 1 slated to perform a high LEO mission, raising its orbit after release from a lower orbit. This CubeSat carries propulsion for the altitude raising and attitude control. The concept of propulsive attitude control

of a CubeSat has been proposed by Gatsonis et al. (2016) and the concept of orbiting raising by Zhang et al. (2017). The eLEO CubeSat is designed to operate between 200 and 250 kilometers while the LEO CubeSat operates between 450-1000 km. It is critical to design the CubeSats so that internal subsystems will be able to withstand these conditions. This is especially important for the eLEO CubeSat which will be subjected to large thermal loads due to the increased atmospheric drag. The LEO mission requires orbit raising and an orbital rendezvous after release at an altitude of about 450 km. As such a large quantity of fuel is necessary due to the complexity of the designed orbital maneuvers, resulting in a large non-conventional CubeSat.
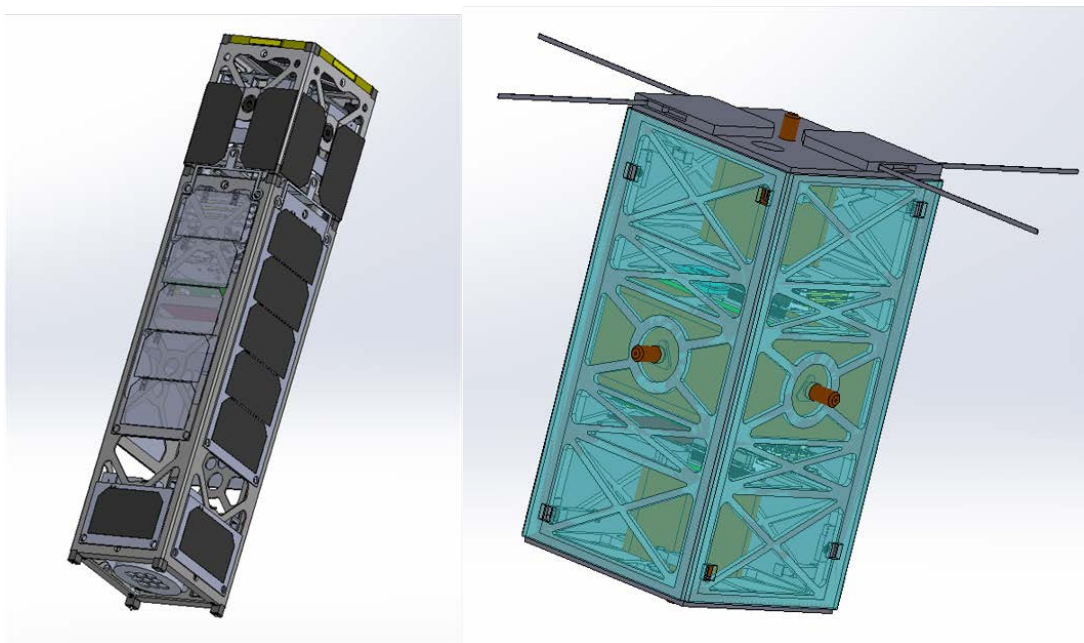
Figure 1: The 4U eLEO CubeSat (Left) and 16U LEO CubeSat (Right).

The goal of this MQP is to perform the mechanical design and thermal analysis, to meet mission requirements for both the 4U eLEO CubeSat and the 16U CubeSat. The second goal is to perform orbital analysis and evaluation of deorbiting time. The third goal is to assess the potential impacts

of magnetic fields induced by magnetic torquers which are considered as alternative candidates for attitude control on the CubeSats.

1.1 Overview of CubeSat Missions

The CubeSat program between Stanford University and California Polytechnic Institute (Cal Poly) in the fall of 1999 was based on a picosatellite OPAL, which was designed by Stanford and had nominal structural dimensions of 4x3x1 inches (Clarke, et al., 1996). Learning from this mission, the optimal design of a cube that was 4 inches per side was conceived, allowing "room for the solar panels and room to contain the cube on some rails in a launcher tube" (Heidt, et al., 2001). For the initial CubeSat design, the launcher tube was decided to hold 3 cubes maximum. This initial launcher would later become the basis for the Poly Picosatellite Orbital Deployer (P-POD) used currently. This collaborative effort which began with Stanford's designs for OPAL would fall to Cal Poly to complete "the launcher design, build a prototype and evaluate for improvements" (Heidt, et al., 2001). Due to this successful design the CubeSat program was announced to many organizations and educational groups as a standardized design for low cost picosatellites (Heidt, et al., 2001).

The first batch of CubeSats were launched on June 30, 2003 on a Eurockot LV from Plesetsk, Russia. Included in the first group were single CubeSats from Japan: the CUTE-I by the Tokyo Institute of Technology and the XI-IV by the University of Tokyo, Canada: the CanX-1 by the University of Toronto, Denmark: the DTUsat by the Technical University of Denmark and the AAU CubeSat by Aalborg University and a triple CubeSat from the United States: the QuakeSat by Stanford University and Quakesat LLC. These CubeSat missions' space-tested key technologies such as deploying solar cells, taking pictures using cameras, testing sun sensors, magnetometers, magnetorquers, communication devices and measuring angular velocities and

acceleations. One specific mission for the QuakeSat CubeSat was detecting ELF radio emission of seismic activity during earthquakes to try and forecast major earthquakes. This group of CubeSats were the first of many to come (Michael, 2009).

Nearly 800 CubeSat missions have launched to date; 295 CubeSats were launched in 2017 alone (nanosats.eu). These numbers will further increase in the coming years. It is predicted that there will be 700 CubeSat missions in the year 2023 (nanosats.eu). CubeSats are typically piggy backed onto larger missions due to their small size and lightweight. Their low cost and ease of manufacture lets engineers design missions to test new technologies or techniques (ISIS, 2018). It is hard to pinpoint an exact cost of launching a CubeSat into orbit. Given the relatively low number of data points available and the rapid pace at which CubeSat technology has been advancing, making estimates more accurate than an order of magnitude is impractical.

Several groups have attempted to quantify this average cost. In 2009, Jos Heyman of SatMagazine analyzed available data to give an estimated cost for launching an educational CubeSat (Heyman, 2009). These satellites were developed primarily by universities and alumni as educational opportunities and launched as secondary payloads on low earth orbit vehicles provided by Russian companies including Eurokot (Heidt, et al., 2001). Heyman's analysis indicated that the full development from inception to space would cost around $52,000 USD as of 2009. A more recent analysis by NASA for general CubeSat development and launch shows that costs are trending down. The Ames cost model developed by Tommy Paine indicates that the total costs are estimated around $14,000 USD as of 2015.

CubeSats have been used to field-test a number of technologies and techniques. The University of Washington's CubeSat platform for ionospheric modelling developed two mission designs that were based on two instrument packages. The objective for these missions was to take distributed measurements in the ionospheric plasma in order to understand density structures and therefore

15

create more accurate models. A second objective was to test to the option of using CubeSats for senior-level aerospace design capstones (Waydo, 2002). Another such mission is the Optical Communication and Sensor Demonstration CubeSat, which launched in 2015 and aimed to field-test the ability of a 1U CubeSat to relay information using lasers (Buck, 2015). This was a part of a series of launches assessing the applications which CubeSats can be useful. This series of tests also included a formation flight test which prototyped water-based propulsion. NASA has also designed a CubeSat to gather weather data and demonstrate the reliability of CubeSats to gather and relay this data. This technology demonstration was meant to show the ability of small satellites to replace large, expensive weather satellites (Blumeberg, 2017).

Universities are not the only group interested in utilizing CubeSat technology for space missions. Government entities such as NASA, NOAA and the ESA have taken to using CubeSats for a variety of space missions. Additionally, the NOAA has contracted two private sector companies, GeoOptics and Spire Global, to build CubeSats to help the NOAA determine the quality of its weather data and forecasts (Voosen, 2016). Prior to this contract the NOAA built and designed its own CubeSats. This sets a precedent for the future as government agencies come under pressure from congress to utilize the private sector to expand into commercial weather satellite options (Voosen, 2016). This move to the private sector will spurn a period of growth for the myriad of companies that produce commercial off the shelf (COTS) CubeSat products. From the conception of the CubeSat program back in 1999, there has always been the mentality that CubeSats should be able to be efficiently designed and built using COTS products.

1.2 Review of Previous CubeSat MQPs at WPI

WPI has been active in CubeSats with undergraduate team projects and graduate research. During the 2011-2012 academic year WPI coordinated with NASA's Goddard Space Flight Center

and the Polish Academy of Sciences to develop a CubeSat that was capable of carrying a spectrometer for scientific analysis of solar and extraterrestrial X-rays. The SphinX-NG CubeSat was designed to enter a polar, sun-synchronous orbit at an altitude of 450-650 km where it's on board spectrometer would be used to collect data. Teams were tasked with the completion of orbital analysis, structural analysis, magnetic field analysis, and mechanical design. In 2012-2013 the Sphinx design was expanded upon and completion of the design occurred in the 2016-2017 academic year. To complete analysis of the Sphinx, COMSOL was used for thermal and magnetic modeling in conjunction with System Tool Kit (STK) to collect orbit data such as Sun and Nadir vectors. Structural analysis was completed utilizing ANSYS and all mechanical design was completed using SOLIDWORKS.

The 2011-12 group had 3 teams with 16 total students. Dopart et al. (NAG-1102, 2012) conducts an orbital decay analysis using Systems Tool Kit, shows the selection of the GPS and the magnetometer, examines a preliminary environmental analysis using COMSOL, and discusses the command and data handling and the on-board computer for the CubeSat. Farhead et al. (MAD-D11A, 2012) presents the hardware selection for the CubeSat, discusses attitude determination algorithms, and describes control policies. Bauer et al. (JB3-CBS2, 2012) conducts a preliminary thermal analysis, and discusses component and assembly design. The group also conducts preliminary stress analysis and discusses power generation and management.

Another CubeSat deign project was conducted during the 2012-2013 academic year by three teams. Billings et al. (NAG-1204, 2013) conducts and orbital analysis in STK, conducts an analysis of electromagnetic interference caused by magnetorquers, and describes the mechanical design. Dawson et al. (MAD-2013, 2013) discusses the production of a test bed for use in testing attitude control methods, and provides selections for sensors, actuators, and computational hardware.

Hanley et al. (JB3-CBS3, 2013) describes the thermal environmental analysis, telecom design, power budget, and a wiring diagram for the CubeSat.

The most recent CubeSat design was during the 2016-2017 academic year. This was a major redesign of to the SphinX-NG design, which was to be placed in a polar, sun synchronous orbit. Curci et al. (NAG-1701, 2017) presents the mechanical design, structural and mechanical analysis, and orbital analysis of the Sphinx-NG CubeSat in addition to random vibration testing done on the frame. Ko et al. (JB3-1701, 2017) discusses the electrical power subsystem, telecom and data handling, and thermal control subsystems for the CubeSat. Agolli et al. (MAD-1701, 2017) discusses the design of the attitude determination and control subsystem, provides simulations for detumbling maneuvers, and created a prototype test bed to test attitude control systems.

1.3 Overview of Subsystems

This MQP is part of a 16-student group of undergraduates which performed mission analysis and design of the eLEO and the LEO CubeSat missions and spacecraft. The students were split into three MQP teams advised by three faculty advisors who also served as the subsystem lead engineers. Furthermore, two graduate students provide lead-engineer functionality along with the faculty advisors. Each MQP team was assigned majors subsystems, organized as follows:

- Orbital Analysis; Mechanical Design; Thermal Analysis; and Magnetic Interference Analysis (this MQP)

- Power; Telecommunication; Propulsion (JB-1801).

- Structural Analysis; Attitude Determination and Control; Command and Data Handling (MAD-1801).

The MQP teams worked separately on their respective subsystems, discussing progress and sharing critical information at weekly Systems Engineering Group (SEG) meetings. The MQP

teams used identical software tools to ensure flawless transfer of technical data. In this manner, the design of each CubeSat evolved to incorporate better methods and components or overcome flaws.

1.4 Objectives and Approach

The first goal of this MQP is to perform the mechanical design and thermal analysis for both the 4U eLEO CubeSat and the 16U CubeSat. The second goal is to perform orbital analysis and evaluation of deorbiting time. The third goal is to assess the potential impacts of magnetic fields induced by magnetic torquers onboard the CubeSat. The objectives and approaches used to meet these goals are outlined below.

1.4.1 eLEO CubeSat

1) The eLEO mission involves a CubeSat which upon release at about 400 km, lowers its orbit below 250 km and remain at extreme low LEO altitudes for as long as possible using onboard propulsion.

   a) Use SolidWorks and a 3U CubeSat model with components from the SphinxNG design (MQP NAG1701) to assess its viability as a platform for the eLEO mission.

   b) Use initial design requirements and parameters for parts, sensors, and subsystems from the SEG teams and develop an initial 4U CubeSat baseline model.

   c) Iterate to accommodate the main propulsion and the pulsed plasma thrusters (PPTs) used for attitude control, maximizing surface area to accommodate non-deployable solar panels for power generation.

   d) Refine the 4U design and update parts, sensors and subsystems as they become available from the other SEG teams.

2) Perform Thermal Analysis

a) Evaluate the thermal environment and heat loads encountered by the 4U CubeSat in eLEO. Generate a de-featured CAD model and import into COMSOL.

b) Use STK to generate data on sun and nadir vectors for a typical orbit as functions of time to obtain unsteady solar heat flux profiles.

c) Use COMSOL's Multiphysics Radiative Heat Transfer Module, and perform unsteady simulations to obtain estimates of the temperature distribution throughout the CubeSat.

d) Assess if temperature of CubeSat components remains within specified tolerances.

3) Perform Induced Magnetic Field Analysis and Assess Possible Impacts.

a) Import into COMSOL the de-featured CAD model used in thermal analysis.

b) Use COMSOL's magnetostatics module, magnetic fields, no current, and model the magnetic torquers as a static source of magnetic flux.

c) Perform EM simulations to obtain estimates of the induced static magnetic field throughout the CubeSat.

d) Assess possible interference with the magnetometers onboard.

4) Perform Orbital Lifetime and Deorbit analysis

a) Use STK to evaluate de-orbit characteristics and lifetime.

1.4.2 LEO CubeSat

The LEO mission involves a CubeSat designed to perform an orbit raising maneuver using onboard propulsion from about 450 km to a higher altitude and subsequently perform rendezvous or formation flying. The objectives and approach are as follows:

1) Perform mechanical design using SolidWorks

a) Use SolidWorks and generate a non-conventional CubeSat design to accommodate the six main thrusters, PPTs for attitude control, and propellant required to perform high-fuel cost orbit raising and rendezvous maneuvers.

b) Iterate to accommodate the subsystems, maximizing surface area to accommodate non-deployable solar panels for power generation. This was accomplished through iterations of increasing satellite size, until power generation and propellant mass were sufficient.

c) Integrate and update parts, sensors and subsystems in SolidWorks from the JB1801 and MAD1801 groups.

2) Perform Thermal Analysis

a) Evaluate the thermal environment and heat loads encountered by the 16U CubeSat under LEO conditions. Use STK to generate data on sun and nadir vectors for a typical orbit as function of time.

b) Generate a defeatured CAD model and import into COMSOL.

c) Use COMSOL's Multiphysics Radiative Heat Transfer Module, module and perform unsteady simulations to provide estimates of the temperature distribution throughout the CubeSat.

d) Assess if CubeSat components temperature remains within specified tolerances.

3) Perform Induced Magnetic Field Analysis and Assess Possible Impacts.

a) Import into COMSOL the defeatured CAD model used in thermal analysis.

b) Using COMSOL's Magnetostatics magnetic fields no current module, model the magnetic torquer as a static source of magnetic flux.

c) Perform EM simulations to obtain estimates of the induced static magnetic field throughout the CubeSat.

d) Assess possible interference with the magnetometers onboard.

21

4) Perform orbital lifetime analysis.

   a) Identify within Systems tool kit the most accurate atmospheric model.

   b) Calculate frontal drag area.

   b) Using Systems tool kit calculate the orbital lifetime of the CubeSat.

2 Mechanical Design

In this chapter, we present the mechanical design of the eLEO and LEO CubeSats. Each CubeSat mission followed its own independent mechanical design process due to their different mission requirements. The eLEO design was initially based largely on the SphinxNG 3U CubeSat (NAG1701) but evolved into a 4U to accommodate the required solar panel area needed to power the necessary attitude control components and extend mission life. The LEO mission CubeSat required a unique frame design rather than one that is commercially available in order to accommodate the additional thrusters as well as the standard instruments and subsystems. The evolution of the SolidWorks designs sand progress was shared in the weekly SEG meetings to receive feedback and inputs for parts, sensors, and subsystems to undergo the necessary revisions

2.1 Design of eLEO CubeSat

2.1.1 Design Drivers

The design process was driven by a number of key factors and requirements. As an initial baseline design, we considered the 3U SphinxNG CubeSat (NAG1701). This helped us establish a baseline from which we could build on and adapt to our needs. The SphinxNG contained multiple electronic components and sensors which would be used on the eLEO CubeSat as well.

The leading design requirement was to maximize the available solar panel area. The limited surface area of the CubeSat and geometry of the solar cell used by Clyde forced our team to optimize placement of other components so as to maximize solar panel area. Solar panels could not be deployable due to the low altitude of the orbit and the drag that the deployable panels would have created. This meant that all power generation had to be done on the surface of the spacecraft and made solar panel area a critical design factor.

The second design requirement was to allow for payload volume. While a specific scientific payload had not been identified, the CubeSat was being developed as a platform for a possible eLEO science packages. This criterion was also a driver behind moving to a 4U structure, as the 3U structure could not be adequately powered with the available solar cell area and have room for a payload.

The sun sensors used in attitude determination and control were also required to be uncovered. This was another driver behind the move to a 4U structure. The geometry of the CubeSat made it difficult to both fit the required sun sensors in the designated locations and have adequate power delivered. Finally, the Pulsed Plasma Thrusters (PPTs) needed to be placed so as to maximize the torques produced without interfering with the solar panels or the solar sensors.

The CubeSat was to use as many commercial off-the-shelf (COTS) parts as possible, but as specific design needs of the CubeSat were identified the geometry of the satellite became more complex. Due to the complexity of some parts, custom fabrication needs were identified with regards to structure. For example, we did not have access to a commercially available 4U CubeSat structure. As such, Pumpkin Inc. was consulted as to whether a 3U to 1U adaptor could be theoretically designed and integrated into the model. After obtaining confirmation that such a part could be designed, and receiving a price estimate of $10,000, the team designed a part that would serve the needs of mating the two parts together and not impede function (Pumpkin Inc., Personal Communication, 2017).

2.2 Design Process

Design features and recommendations were discussed in the weekly SEG meeting. Each SEG team would present the week's findings, open tickets, and recommendations. Early in the project, the teams also established lines of communication with each other to pass along design information

as quickly and efficiently as possible. Teams also met with their advisors as well as their assigned graduate student lead engineers on a weekly basis.

Starting with the SphinxNG components, the design group attempted to integrate parts in such a way that satisfied the mission requirements. A slideshow presentation was made documenting the week's changes and the model for the week was saved using SolidWorks *Pack and Go* feature. This feature saved the entire assembly as a zip file with the name "eLEO CubeSat" followed by the design iteration number. This let the team keep a detailed documentation of week to week changes. A parts list was also updated for parts which had been added that week. Below is our initial CubeSat design in Figure 2.
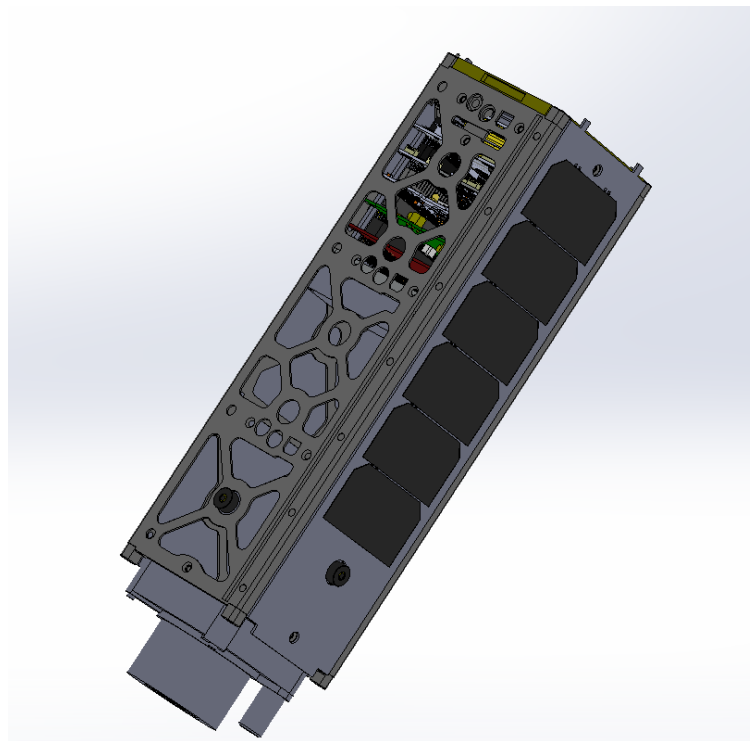
Figure 2: The initial CubeSat model for eLEO mission.

Several challenges were faced during the design process. After the initial 3U design was proposed it was determined that the power production during illumination was not sufficient to recharge the battery completely. This caused the CubeSat to completely shut down during eclipse.

Additionally, with the required sun sensors for orientation and attitude determination, additional solar panels could not be attached to the chassis.

To address this issue, a 3U chassis was attached to a 1U chassis to create an ad-hoc 4U, using a custom connection part which would be manufactured, shown in Figure 3. This allowed for an increased solar panel area to a degree which was able to recharge the battery and keep the CubeSat powered through the eclipse phase. This made a design that could not adhere to the P-POD standards CubeSat which require a maximum length of 340mm along the Z axis (Kramer, 2018).
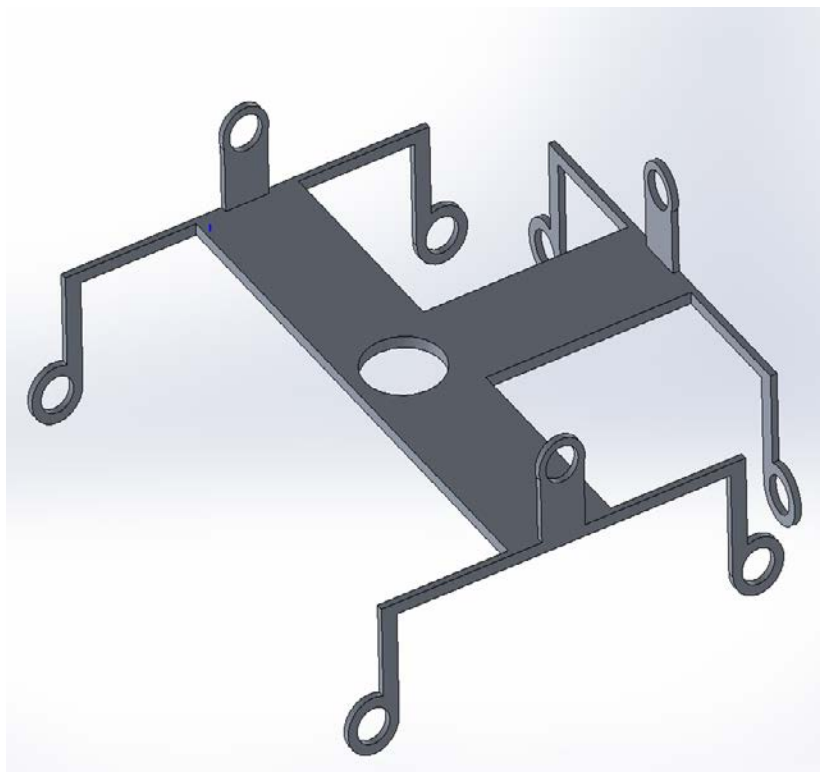
Figure 3: The eLEO CubeSat chassis connector model.

Another issue faced was a lack of available models for required parts. The Busek thruster shown in Figure 4 which was selected for main propulsion did not have an available model and was designed to resemble photographs as much as possible. Additionally, it was decided to house the engine inside the chassis to reduce the overall length of the model, so a mounting system was developed which would attach to the existing geometry of the chassis and hold the engine in place.

BET-1mN Electrospray Thruster

Precision Miniature Valve
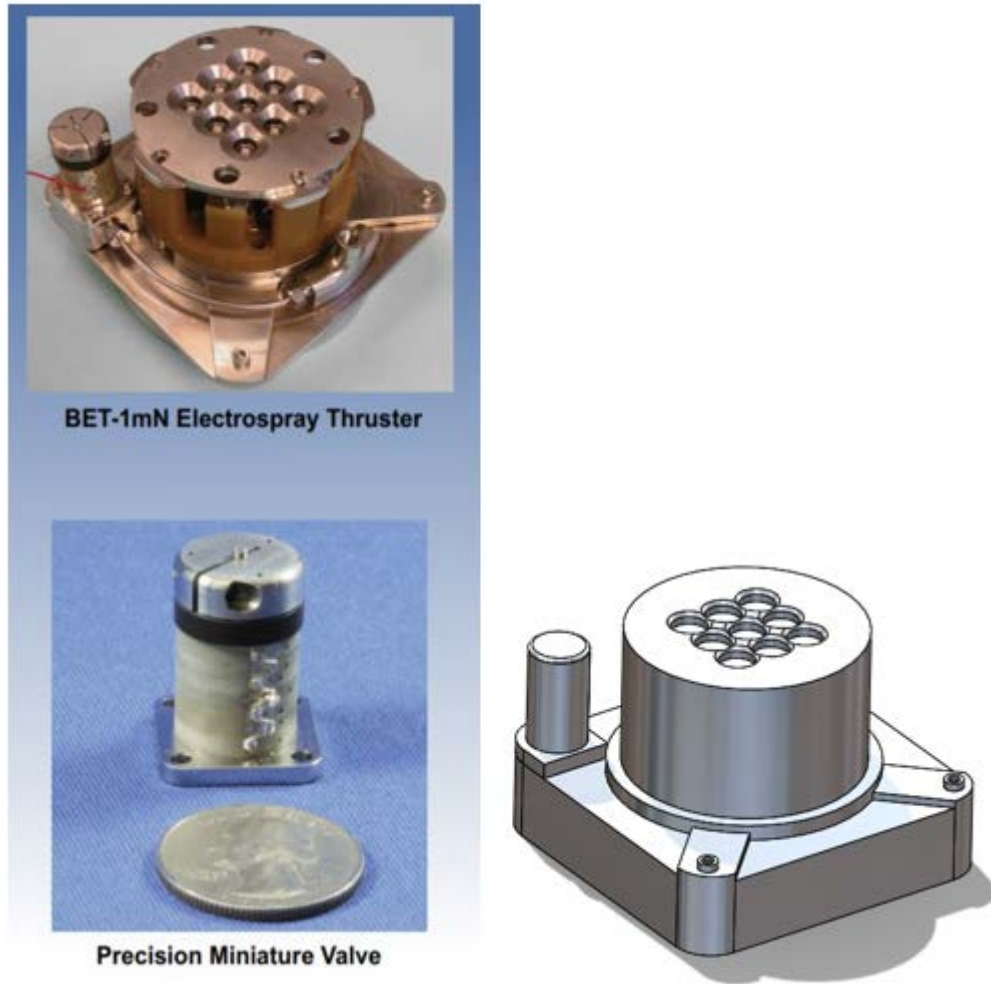
Figure 4: The reference images for the Busek thruster obtained from busek.com.

While creating the final assembly, attention was paid to ease of construction. Mounting holes were aligned with existing geometry present in the chassis as much as possible, and side of the chassis which opens to allow assembly was left unblocked. This was done to create an assembly that was as realistic as possible for analysis and component selection.

Several areas on the CubeSat were made more efficient over the course of the project. Initially the CubeSat used 4 Coarse Sun Sensors and 1 Fine Sun Sensor. It was later determined that the Fine Sun Sensor exceeded the mission requirements to such a degree that a Coarse Sun Sensor could also satisfy the mission need. This allowed for easier integration into the architecture of the

CubeSat and reduced the weight of the overall model. Another area of refinement was the switch to Pulse Plasma Thrusters for attitude control rather than the baseline magnetorquers. Though this required changing the solar panel design slightly, it allowed for finer and stronger attitude control.

2.3 Summary of Mechanical Design

The final 4U CubeSat assembly shown in Figure 5 addresses the design and technical requirements necessary for the mission to operate for as long as possible in an extreme Low Earth Orbit environment. The design choices reflect the need to meet these mission requirements, however there were a few decisions that represent the most important choices. As a result of the design process, maximum solar panel area was a foremost necessity so that the battery could recharge completely and maximize mission life. In addition, PPTs were chosen over magnetorquers or reaction wheels as instantaneous attitude determination and control is needed to maintain steady orbital flight.
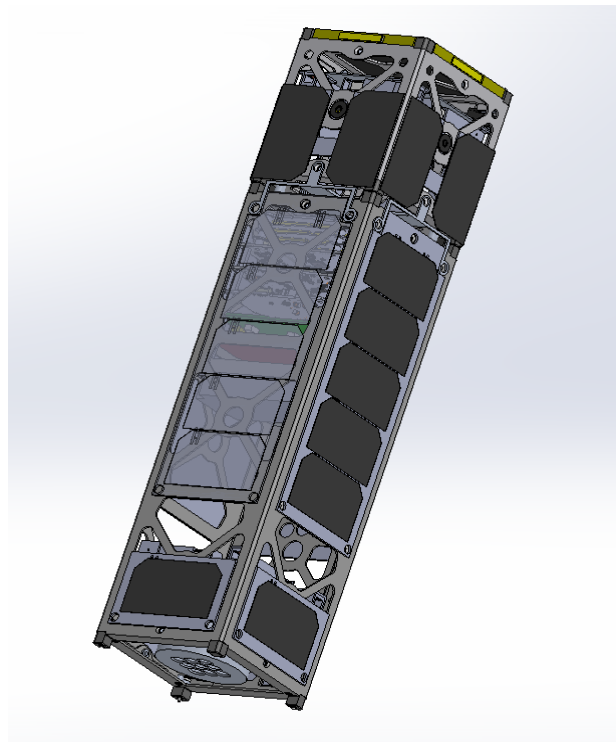
Figure 5: The final eLEO 4U CubeSat design.

Table 1 provides a list of the components for the 4U CubeSat assembly.

Table 1: List of eLEO CubeSat Components

Parts	Quantity	Manufacturer
4U Chassis	1	Pumpkin
Busek Electrospray Thruster System	1	Busek
1 Panel Solar Panel-custom	1	Custom Construction
2u Solar Panels-custom	3	Clyde Space
Coarse Sun Sensor	4	Space Micro
Gyroscope	1	analog devices
OBC(On Board Computer)	1	Clyde Space
Magnetometer	1	New Space Systems
3rd Gen 3U EPS(Electrical Power System)	1	Clyde Space
40 Whr Battery	1	Clyde Space
Deployable Antenna System (ISIS)	1	ISIS
ISIS TRXUV VHF/UHF Transceiver	1	ISIS
SGR-05U - Space GPS Receiver	1	Surrey Satellite Tech
Pumpkin CubeSat Kit Protoboard	1	Pumpkin
Circuit Stack Base	1	
Micro PPTs for ACS	8	

2.4 Design of LEO CubeSat

2.4.1 Design Drivers

The main design challenge to overcome for the LEO mission was the need of custom CubeSat frame to accommodate six main thrusters while maximizing surface area to ensure that enough power is generated by surface mounted solar arrays. CubeSat structures consisting of 8U, 9u, 12U, 16U and 20u were considered to meet critical mission requirements. In the end it was decided that a 16U structure would be the baseline design. The 8U, 9u and 12U designs were scrapped early on due to not having enough internal volume to accommodate enough fuel for 6 thrusters and have enough surface area for solar arrays.

The primary task of the LEO design team was finding a way to fit enough propellant into the structure while having enough room left over for the remaining subsystems. As a baseline each thruster required 1U for the hardware and propellant tank. The center of mass was designed to be as close to the geometric center of the 2x2x4U structure as possible. In line with this goal the design was made as symmetric as possible. Items without duplicates were placed in such a manner as to maintain the center of mass as best possible. The CubeSat needed full 6 axis control, to this end pulsed plasma thrusters (PPTs) were used for attitude control. Other methods of attitude control considered were magnetorquers and reaction wheels. The CubeSat required a large quantity of power to run, body mounted solar panels were designed to cover as much of the available surface area. Deployable panels were undesirable because the panels would stand a chance of being damaged by the PPT's, or main thrusters during mission operation.

Each face of the CubeSat is equipped with a sun sensor to assist in Attitude determination, these had to remain visible to function. Two types of sun sensor were used, a fine and a coarse sensor. Placement of an antenna was problematic, most CubeSats are designed to have a full open face on which to mount the antenna, but the logical positions on the LEO CubeSat were taken by thruster nozzles.

2.5 Design Process

The basis of the LEO design rests on the custom chassis, this chassis consisted of multiple panels assembled after internal components were in place. The entire 16U design rests on the main frame structure, shown in Figure 6. The side and top frames attach as shown in Figure 7.
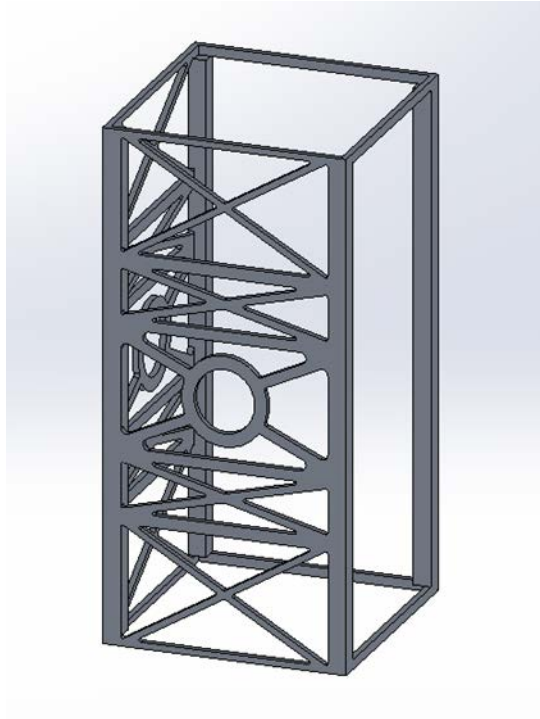
Figure 6: The 16U main frame design.
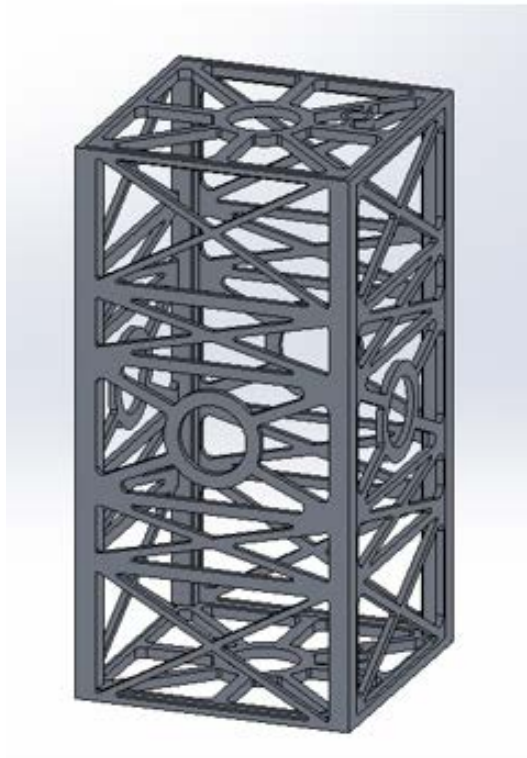
Figure 7: The 16U auxiliary frame design.

The top and bottom panels also contain two sections used to mount sun sensors, these are smaller holes off to the side of the main thruster hole. Interior floors were added to allow internal mounting and separate the four central thrusters from the circuit stack. The interior floors can be seen in Figure 8.
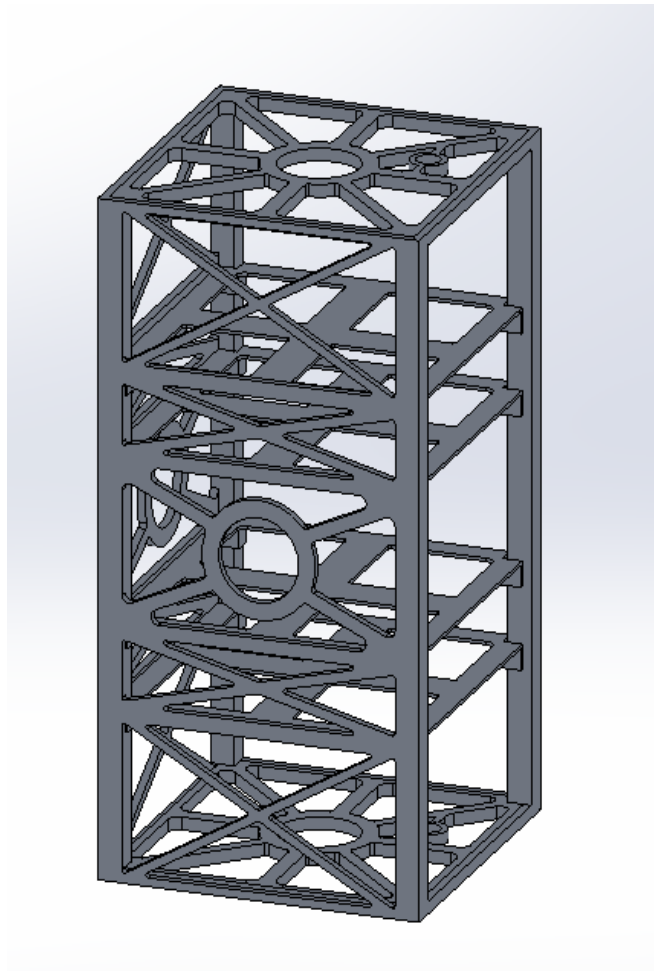
Figure 8: The 16U internal truss system.

The main thrusters and PPT's were added to provide full six axis control of the CubeSat. Thrusters were positioned to have 3-axis control to establish formation flight during the CubeSat's orbit. In order to keep the center of mass as close to the geometric center of the 16U, 2 thrusters were placed along each body axis. Pictured below is the layout of the thrusters within the 16U frame. Their positions are shown in Figure 9.
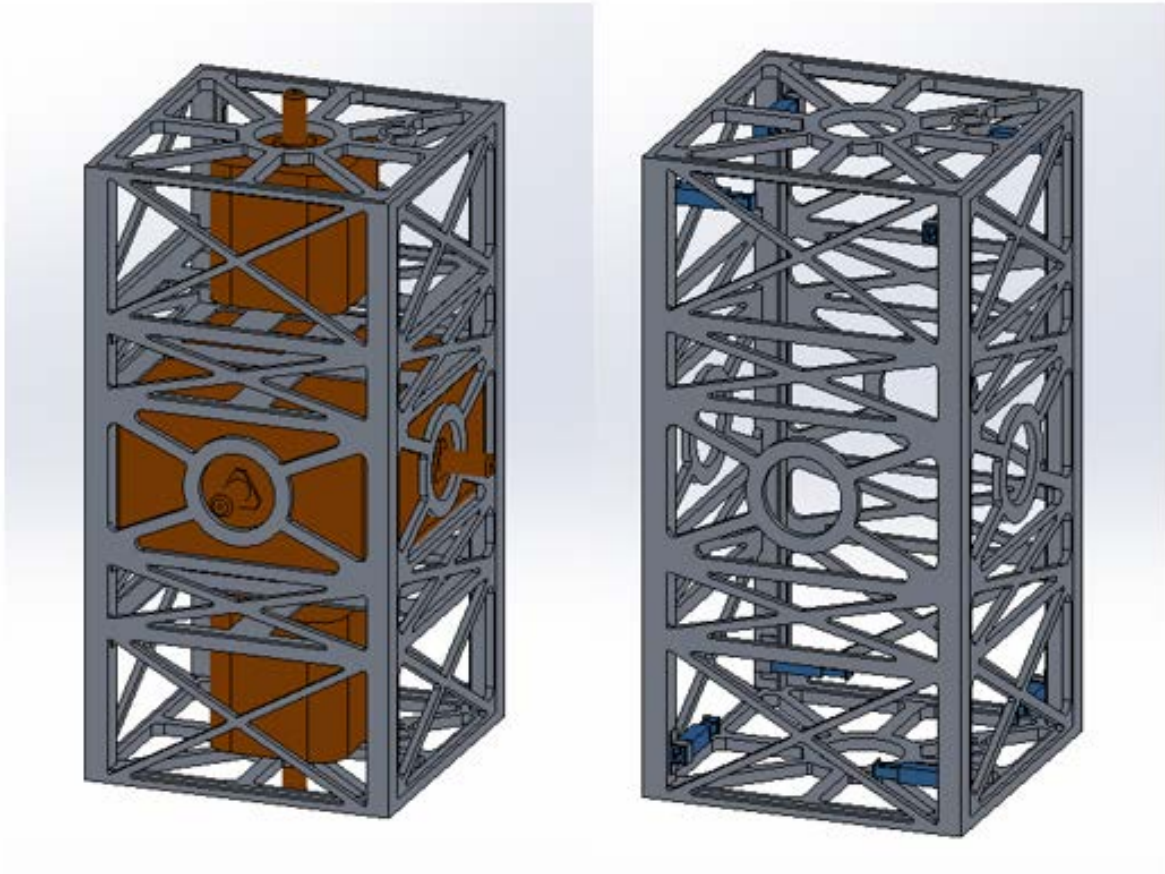
Figure 9: The main thruster locations (left) and PPT locations (right).

It was apparent that commercial off the shelf propellant tanks were not available to accommodate our design. A fuel tank was designed that would feed 4 center thrusters and was positioned in the center of the 16U frame. 2 thrusters were then positioned at the top and bottom of the craft for along with their respective fuel tanks. The PPT's were designed to fire in clusters to allow rotation in any direction, the clusters that would fire for each rotation are shown in Figure 10 and Table 2. Note: PPT's #4 and #8 are not visible but their direction is indicated.
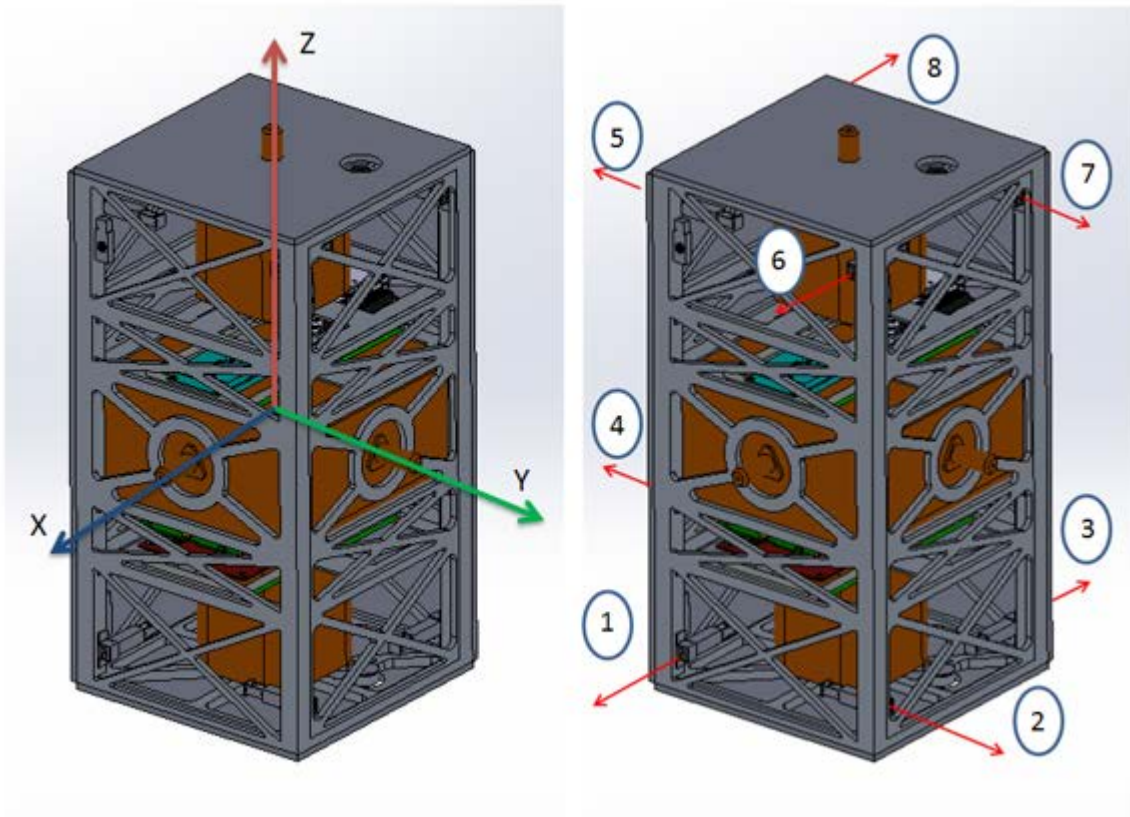
Figure 10: The PPT positions and firing directions.

Table 2: PPT Control Clusters

Rotation	Thrusters
Clockwise X	2,5
Counterclockwise X	4,7
Clockwise Y	1,8
Counterclockwise Y	3,6
Clockwise Z	5,6,7,8
Counterclockwise Z	1,2,3,4

Sun sensors were added to every face of the CubeSat to aid in attitude determination, two types were used. The fine sun sensor and the coarse sun sensor. These can be seen in the design in Figure 11.
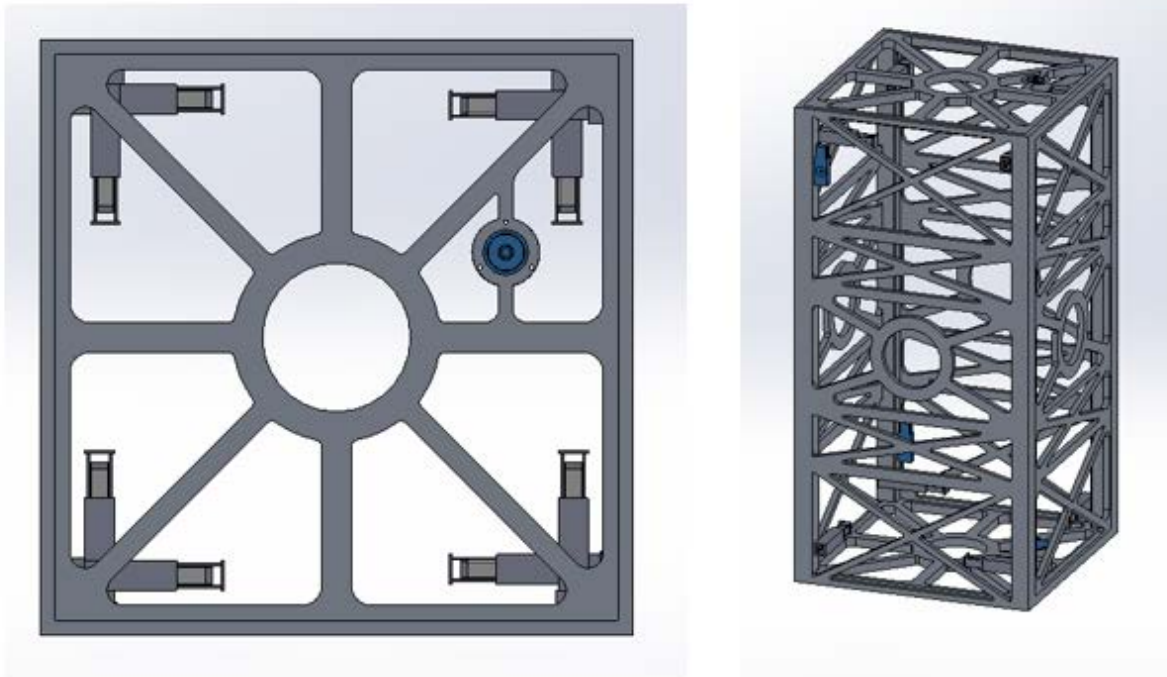
Figure 11: Locations of fine and coarse sun sensor (shown in blue).

Another design challenging was fitting all of the on-board computer systems in the 16U frame. Unlike the eLEO CubeSat design the LEO CubeSat would not be able to have a traditional control stack that would fit within 1U of internal volume. Instead all of the electronics for onboard systems were separated and placed above and below the center section of thrusters and fuel tank. Normally the control stack is integrally powered with a battery located on top of the stack to power its electronics. Separation of the control stack facilitated the need for a non-COTS wiring harness. The design of the electrical harness was not considered, but it should be mentioned as a tradeoff with the 16U design. The locations of the circuit stack, and other internal electrical components can be seen in Figure 12.
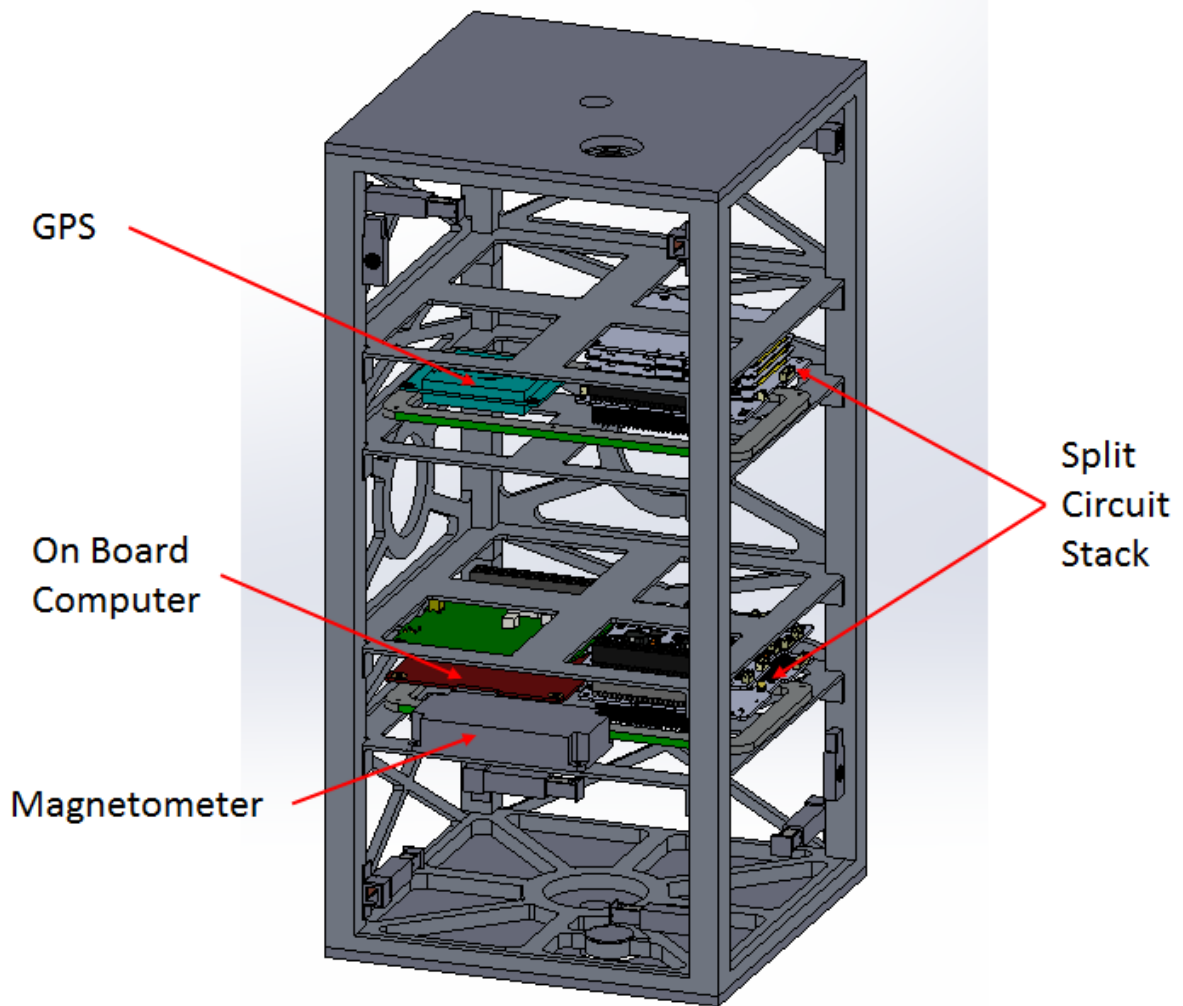
Figure 12: The position of internal electronic subsystems in the 16U CubeSat

To generate enough power for the mission the 16U CubeSat needs to have as much of its surface area covered as possible. To accomplish this unique solar panels would need to be designed. Currently there are no commercial off the shelf solar panels that could be direct purchased to meet mission requirements. This fact drove the need to design simple solar arrays that would cover the 16U frame. Simple models of what these solar panel would look like were created and placed on the 16U frame in SolidWorks. The main requirement for these panels is to not interfere with thrusters, PPTs and sun sensors housed on the 16U frame. Holes had to be made for these onboard systems. Seen below, in Figure 13, are simple models of the solar panels designed for the 16U.

Figure 13: The 16U simplified solar panel model.

The antennas used on the 16U are modified versions of the antennas used on the eLEO CubeSat. There is no commercially available antenna that can directly meet the needs of the 16U configuration. The main issue being clearance between the thruster nozzle and antenna while also maintaining line of the sight for the sun sensor placed on top of the 16U. One solution proposed is to use 2 antennas and modify their geometry to ensure that there is clearance with the antenna body and thruster nozzle. Solar panels would then be placed on top of the antenna body to ensure maximum panel coverage. The antennae can be seen in Figure 14.
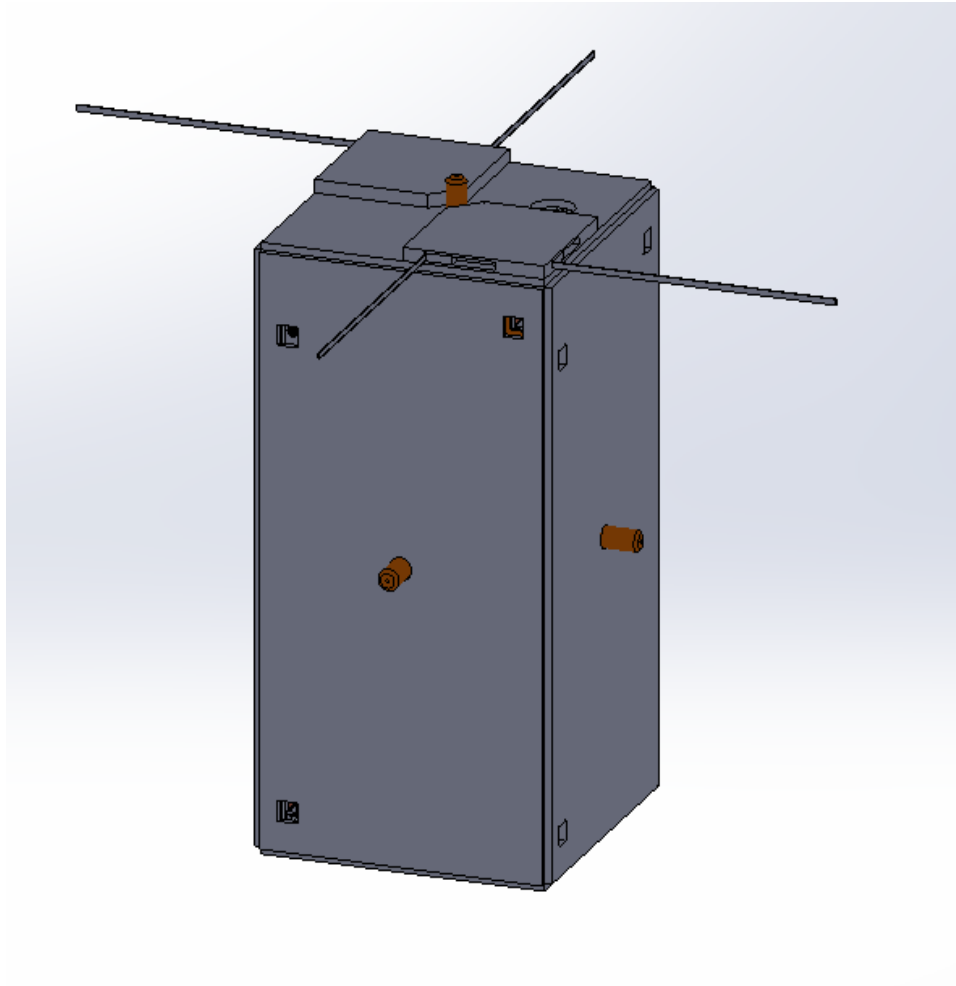
Figure 14: The 16U CubeSat with the modified ISIS antenna.

2.6 Design Summary

Given the unique layout of the design, and the need for several custom-built components, the deployer for the CubeSat would also need to be a custom design. This is to ensure the safety of the thrusters during deployment. The solar panels remain the largest concern, given the power demands during burns, these custom-built panels would have to be thoroughly tested before launch to ensure the PPTs do not damage the panels during burns. Four holes are needed, two for PPTs, one for the sun sensor and one for the thruster.

3 Orbital Lifetime Analysis

In this chapter we present the deorbit lifetime analysis conducted using the Systems Tool Kit's (STK) built-in lifetime feature. With this, STK is able to calculate the time to deorbit given the orbital elements of the satellite, the drag coefficient, and areas of the satellite's faces. The STK lifetime feature considers a satellite deorbited when its orbit falls below 65 km. According to NASA's P-POD requirements, CubeSat's should naturally reenter the atmosphere within 25 years.

3.1 4U eLEO CubeSat Analysis

The first step for modeling the orbital decay of the 4U CubeSat was to provide STK the frontal area of the spacecraft, and the coefficient of drag (which is approximated to 2, as done for most blunt body satellites). The solar radiation pressure coefficient is approximately 1 for most standard spacecraft. This is a measure of how much the sun's light "pushes" the spacecraft and can have a significant effect over long periods of time. The area exposed to the sun and the mass of the satellite must also be provided. Finally, an atmospheric model must be selected. The model determined to be the most accurate was the NRLMSISE 2000 model, which was developed by the US Navy based on empirical data on high altitude ion densities. This model provides the most accurate measure of high atmosphere ionic oxygen (known as "Anomalous Oxygen" in the model), which can play a major role in spacecraft drag (Picone et al, 2000). The other models available were used to verify the data obtained from the NRLMSISE 2000 model, and check for inconsistencies. Orbital parameters for the eLEO CubeSat are shown in Table 3. The satellite was evaluated for two masses: 2.5 kg, and 4.5 kg. The weight of the model as indicated by SolidWorks was 2.5 kg. However, this did not include fuel, tankage mass, or a payload. Additionally, common convention states that a CubeSat weighs about 1 to 1.3 kg per unit (NASA, 2018). For this reason, a dummy

mass of 2 kg was added. This brought the total satellite mass to a more reasonable 4.5 kg. The decay of the spacecraft's orbit is shown in Figure 15.

Table 3: The eLEO CubeSat Orbital Elements.

Inclination	51.63°
RAAN	352.6°
Eccentricity	.0022
Argument of Perigee	76.15°
True Anomaly	323.7°
Semi-major axis of Target Orbit	6603.1km
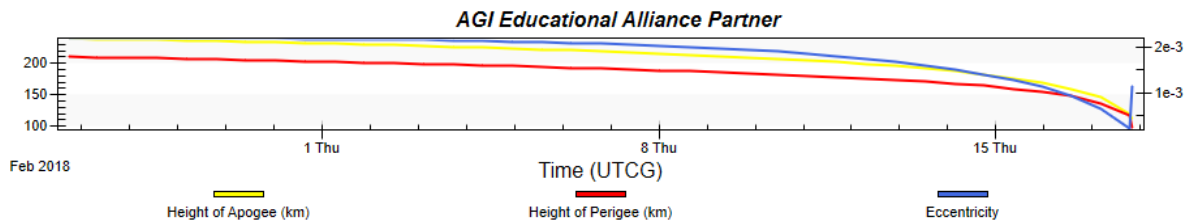
Figure 15: The decay of the eLEO CubeSat orbit shown in terms of the apogee, perigee, and eccentricity.

The CubeSat with the dummy mass had a lifetime of 24 days after engine shut off. This was consistent across all atmospheric models contained in STK ±1 day. Requirements for CubeSats for limiting space debris dictate that a CubeSat must have a maximum lifetime of 25 years. As such, the eLEO CubeSat is compliant with NASA standards.

3.2 16U LEO CubeSat Analysis

For the LEO CubeSat, the same methodology was used as in the eLEO mission. The LEO mission had multiple potential orbits, one was equatorial, one at a 45-degree inclination and one polar orbit. For each of these orbits an analysis was run using the best and worst case atmospheric

drag areas for the CubeSat. The 'worst' case analysis uses a frontal area of 0.048 square meters, and the 'best' case uses 0.088 square meters. This is because the planned mission life is short compared to the possible orbit lifetime thus we want the CubeSat to deorbit faster rather than slower. The mass for both cases and area exposed to the sun are the same, both are kept at 16 kilograms and 0.1 square meters. This is due to the one kilogram per unit assumption and the fact that the sun tends to hit more than one face of the CubeSat at a time. The STK analysis tool and best case frontal area are shown in Figure 16. The only number to change for the two simulations is underlined in red.
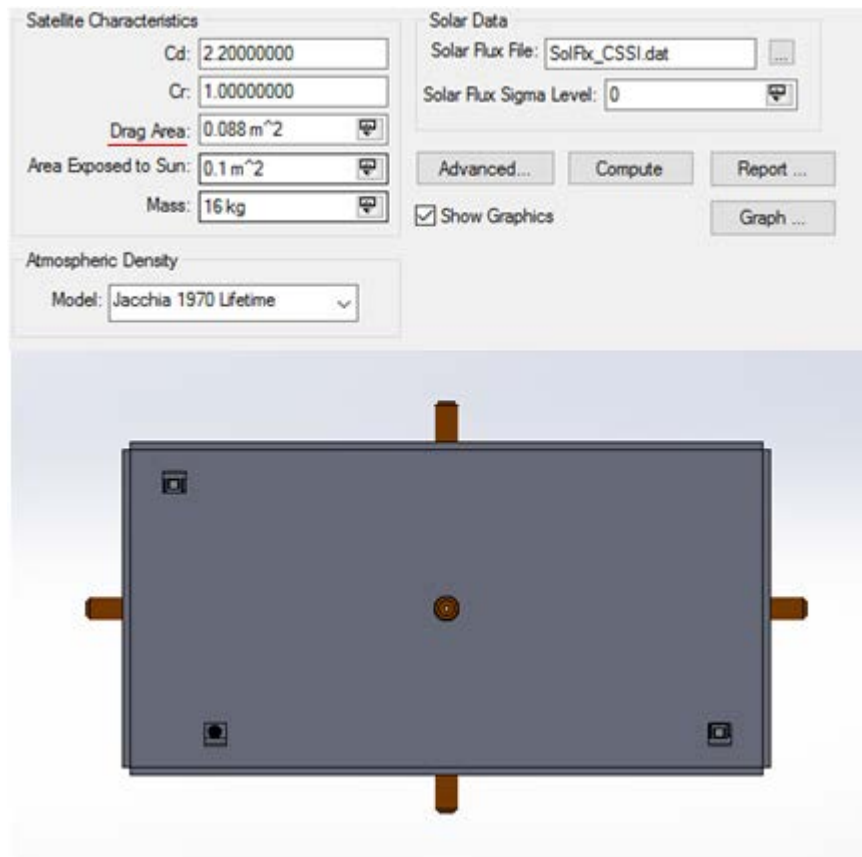
Figure 16: The STK orbital analysis interface, with drag area underlined.

Running the simulation for each of STK's 10 atmospheric density models and each of the CubeSat orbits returns two separate average values for the best and worst cases on each orbit. These total for sixty simulations and once the numbers are averaged out, the expected lifetime of

the CubeSat is between 9 and 16 years. Individual models returned occasional outliers, with some models predicting into the 30-year range and others as low as 5.

It is important to note that the lifetime tool only accounts for the lifetime of the CubeSat's orbit. It does not have any features that detail the safety of deorbiting, or breakup calculations. NASA's Debris Assessment Software is able to accomplish this, but we were unable to gain access to the software. In terms of likely damage, a typical satellite will have 10% to 40% of its material survive reentry. This is lessened if most of the satellite is made of aluminum, which has a lower melting temperature than other common materials used on spacecraft, such as titanium or steel. As the CubeSat frame is aluminum, and all other parts are very small compared to a full-size satellite, the probability of danger associated with deorbiting is slim to none (Aerospace Corporation, 2018). Due to the certainty of breakup, a re-entry plan is not required.

4 Thermal Analysis

In this chapter we present thermal analysis for the 4U and 16U CubeSats. The thermal loads expected during a typical orbit of the eLEO and LEO CubeSats are discussed and evaluated as functions of time in orbit. Thermal analysis is performed using COMSOL Multiphysics Radiative Heat Transfer Module, but due to the extreme computational requirements we used the de-featured CAD modules of the CubeSats. Results are discussed and compared with available temperature tolerances for parts and components of the CubeSats.

4.1 eLEO 4U CubeSat Thermal Analysis

The thermal environment in space is harsh, and a spacecraft can reach temperatures above 100° C in sunlight and drop below freezing during eclipse. The lack of atmosphere makes the sole method of heat regulation blackbody radiation. This means direct exposure to the sun causes intense heating due to radiative heat transfer. These extreme highs and lows for temperatures can cause the sensitive electronics carried by the CubeSat to fail. For this reason, it is important to model as accurately as possible the thermal environment the CubeSat will experience. Both the eLEO and LEO CubeSats use similar electronic components which are listed in Table 9 with their reported temperature range as reported by their manufacturer.

In order to keep the electronics on the CubeSat in their operable temperature range, several methods of thermal control can be utilized. There are two types of thermal control, active control and passive control. Active thermal control with the purpose of cooling usually utilizes a moving fluid to transfer heat from one part of a spacecraft to another which will radiate the heat away (Wright and Dunbar, 2013). This is impractical on a CubeSat due to the mass and complex nature of the subsystems. As such, passive thermal control systems are utilized. One popular passive

cooling technique is using a thermal dissipative/reflective coating. Coatings don't require an entirely separate subsystem and are a popular choice for CubeSats which require cooling.

In eclipse, a CubeSat may require heating if the thermal energy stored in the satellite coupled with the heat produced by the electronics is insufficient to meet the requirements to keep the electronics operational. In this case, electric heaters may be utilized in order to keep the electronics in working order (Thermocoax, Accessed 2018).

4.1.1 Approach

To model the thermal environment the COMSOL Multiphysics Radiative Heat Transfer Module was used. More specifically, the Heat Transfer with Surface to Surface Radiation model was used, which is a subsection of the Radiative Heat Transfer Module. For the eLEO simulation, the environment included a moving solar heating vector in addition to the heating due to atmospheric friction. The Solar Constant, S was assigned a value of 1367 W/m^2, the heat flux of solar radiation at 1 AU. Unfortunately, at the time of this writing, COMSOL was not able to model the heat transfer due to atmospheric friction for Knudsen numbers greater than 1. The Knudsen number relates a particle's mean free path length to a characteristic length; generally, the particle's diameter. At 200 kilometers, Knudsen numbers are greater than 10; this corresponds to an area of gas dynamics known as the free molecular flow regime. Here, the particles are extremely high energy, but the density of particles is extremely low. This meant that COMSOL could not directly model the energy transfer due to the collisions with these particles.

In order to determine the heat flux to the front of the CubeSat due to the free molecular flow, the equation (1) derived in from Gombosi (1984) was used.

$$\Delta\varphi(E) = \frac{\alpha}{4} n_i \bar{v}_i k T_i \left\{ e^{-s\frac{2}{3}} \left\{ s^2 + \frac{\gamma+1}{2(\gamma-1)} - \frac{(\gamma+1)}{2(\gamma-1)} \frac{T_w}{T_i} \right\} \right\} \qquad \text{Eq. (1)}$$

In Eq. (1), $\Delta\varphi$ is the incident heat flux calculated. The variable α is approximated to 0.9 for most spacecraft, while n_i corresponds to the density of incoming particles calculated by MSIS (NASA, 2015). $\bar{v}_i$ is the mean velocity of the incoming particles, which is approximated to be equal to the velocity of the spacecraft); k is boltzmann's constant, and T_i is the incoming temperature of particles at the current altitude. T_w corresponds to the temperature of the spacecraft at a given point. The variable s is a calculated value, the product of the spacecraft speed and the square root of the Mach number divided by $2kT_i$. We made the following assumptions: the CubeSat's front face can be treated as a blunt body flat plate; the CubeSat is traveling significantly faster than the thermal speed of the ambient particles, and the CubeSat deflects or reflects all the particles it encounters.

Using Eq. (1), the heat flux was determined to be 2.44 W/m^2 (Gombosi, 1994). This was significantly less that the solar heating but determined to be significant enough to include in the model. The particle densities to use as model inputs were obtained from NASA's MSIS atmospheric data model (NASA, 2015). The area of the CubeSat's frontward face was calculated in SolidWorks using the evaluation tool. The specific heat ratio γ of the gasses were assumed to be monatomic, and therefore 1.4. The MATLAB file developed to calculate the heat flux is shown in Appendix A.

First, a de-featured version of the SolidWorks model was generated which had significantly reduced detail without sacrificing general geometry. Complex features such as the circuit stack were approximated in general shapes, whereas smaller parts such as the sun sensors were omitted

entirely. This smoothing process was done in SolidWorks. The files obtained from manufacturers contained fine geometry and small holes and cuts which were fractions of a millimeter wide. Screws and machining holes were also included, likely to represent byproducts of the manufacturing process. These were all removed via extrudes and extrude cuts in SolidWorks to reduce the number of elements in the COMSOL mesh. From the first iteration to the last, the number of elements was decreased from greater than 200,000 to less than 30,000. This reduced the time of running one computation from over an hour to roughly seven minutes. Comparisons of the de-featured models are shown in Figure 17 and Figure 18.

Figure 17: The de-featured 4U CubeSat COMSOL model compared to the unaltered model.
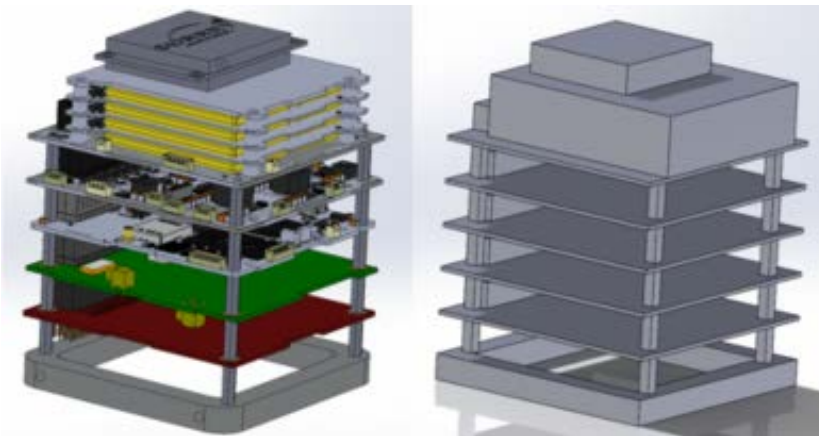
Figure 18: The de-featured 4U CubeSat circuit stack compared to the unaltered model.

Next, STK was used to obtain the luminosity data of the spacecraft. This corresponds to a table

with a timestamp and an output of 100 or 0 (100 meaning the spacecraft is currently illuminated,

0 meaning the spacecraft is in eclipse). Any output value of 100 was changed to 1 for use in

COMSOL, since a value of 1 serves the heat flux equation without changing the magnitude but

still indicates that the spacecraft is illuminated. Next, the sun vector data was recorded. This

corresponded to a table of values which indicated the incidence angle of the sun with one face of

the spacecraft. An example of the luminosity tables is shown in Figure 19.
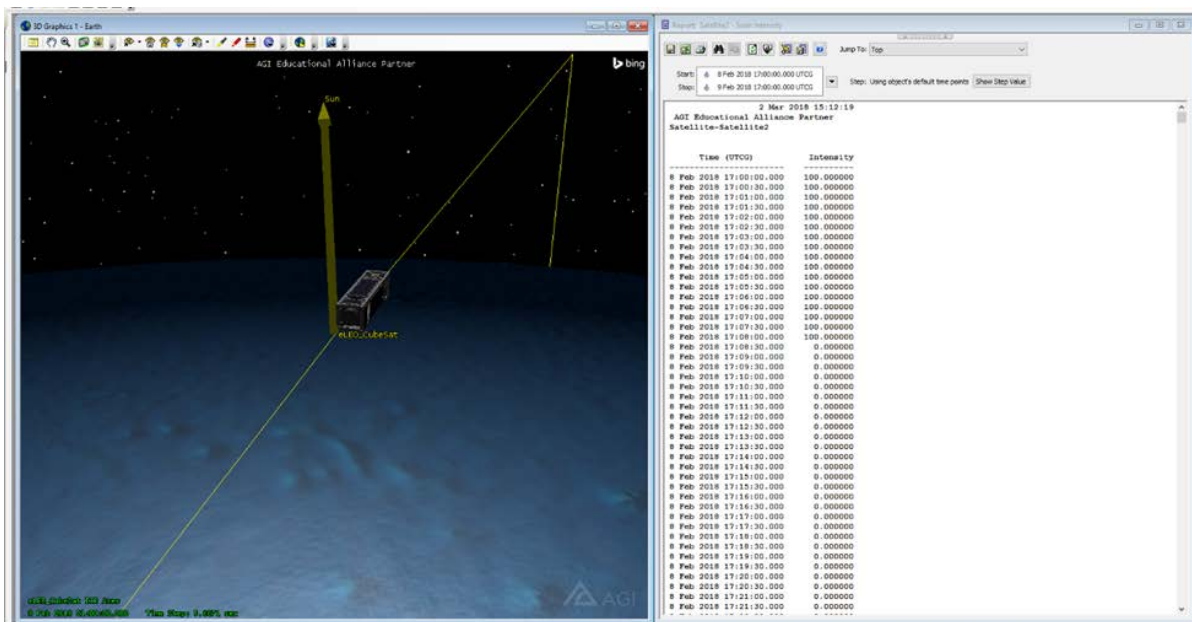
Figure 19: The luminosity tables used in the thermal analysis.

In both data sheets, the time column was changed so that it ranged from 0 to 14400 seconds (4 hours) with a time step of 1 second. This data range was arbitrarily chosen to determine the heating and cooling effects over time. The range of time chosen depends on how long an orbit is run for in STK and is arbitrary. Using both of these data sheets, it can be determined both when the CubeSat is illuminated, and the angle of incidence the sunlight makes on the CubeSat.

Finally, these data were entered into a COMSOL Radiative Heat Transfer simulation. Both the luminosity data and solar incidence angle data were entered as interpolation functions under the Global Definitions tab. Each data source was further entered as a local table in the Definition section of each interpolation function. These functions were later used as part of the solar flux equations; the solar luminosity data was given the variable $SI(t)$ for Solar Intensity and the solar incidence angle data was given the variable $SA(t)$ for Solar Angle. The names of the data sets, and their corresponding variables are shown in Table 4. The periods of illumination and eclipse can be seen in Table 12 in the appendix.

Table 4: Variables used in COMSOL for the eLEO CubeSat.

Data Set Name	Description	Variable
Solar Intensity	Sunlight illumination period	$SI(t)$
Solar Incidence Angle	Incidence angle of sun vector to spacecraft	$SA(t)$

In the Geometry tab, we imported the most simplified CubeSat model as a STEP file. We used geometry tools to smooth the model further and reduce the number of elements. By reducing elements, COMSOL can run the geometric mesh through its equation solvers more efficiently. By using the Repair tool, COMSOL automatically removes small details and repairs defects in the geometry. We also used the Delete Sliver Faces tool; this tool deletes any faces that are smaller

48

than a specified maximum face width. Since the 4U CubeSat has many slim faces, specifically the edges of the solar panels, this tool deleted any edges smaller than 0.001 meters which removed the edges of the solar panels and improved the geometric mesh quality. One automatic function COMSOL performs when a model is imported is assigning domains, boundaries and the selection of Identity Boundary Pairs under the Component Definitions tab. The domains and boundaries specify the various parts, faces, edges and corners on the model, while the pairs effectively tell COMSOL what can radiate heat to another surface in the spacecraft structure. The boundary pair automatic selections are shown in Figure 20.
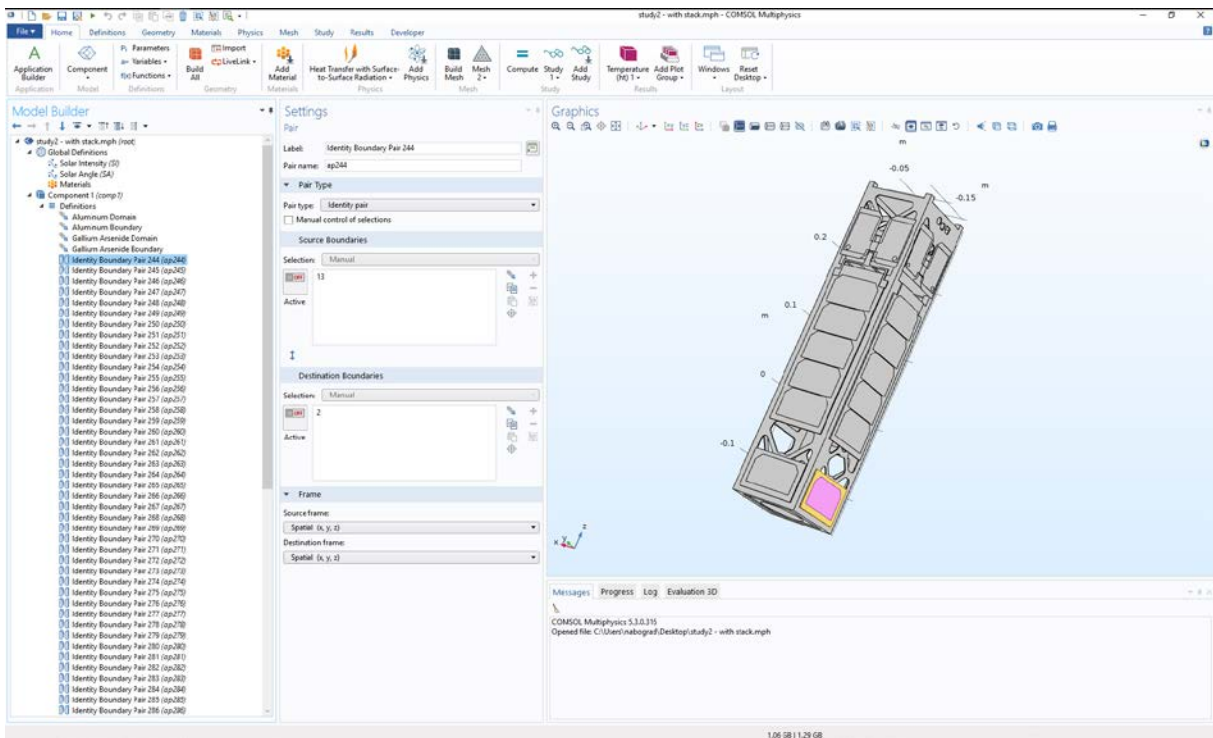
Figure 20: Using boundary pair selection to define the thermal model.

For the next step, specific materials were assigned to each of the domains and boundaries on the model from COMSOL's material library. To simplify the model, only two materials were used. For each solar panel, the material Gallium Arsenide (GaAs) was chosen for all domains and boundaries that belonged to the panels since solar panels are commonly made of GaAs. For the

rest of the model, solid Aluminum 5052-H32 (5052 Al) was chosen for the CubeSat chassis, thruster, solar array backing, circuit stack, and chassis unit connector. Although not all of these parts are composed of 5052 Al, we can assume as a simplification that the heat transfer will behave similarly for 5052 Al in comparison with the specific materials for each part. Both materials required further inputs for Surface Emissivity (ε), which we found was 0.115 for 5052 Al and 0.85 for GaAs. The parameters and their defined variables are shown in Table 5.

Table 5: The defined parameters for the heat flux equation used with the eLEO CubeSat.

Parameter	Variable	Value [Units]
Solar Constant	S	$1367 \ [W/m^2]$
Aluminum 5052-H32 Surface Emissivity	ε_{Al}	0.115*
Gallium Arsenide Surface Emissivity	ε_{GaAs}	0.85*
Surface Emissivity Material Parameters retrieved from (Ko et al., 2017).		

The Heat Transfer with Surface-to-Surface Radiation tab is the primary section for the thermal physics modeling. Settings in the Solid subtab were not set up automatically by COMSOL. In the Opacity subtab, the opacity was set to Opaque so that the radiative heat flux could be opacity controlled. The initial temperature was set at 305 degrees Kelvin (K) in the Initial Values. The Thermal Insulation subtab displayed which boundaries acted as insulation, however many of these were overridden by further heat flux settings. We then selected all of the Identity Boundary Pairs as a Pair Thermal Contact subtab for all the pairs of boundaries. Due to how COMSOL makes Pair Thermal Contacts and because there are limits, numerous Pair Thermal Contact subtabs were made to select all of the Identity Boundary Pairs. The Pair Thermal Contacts can be seen in Figure 21.
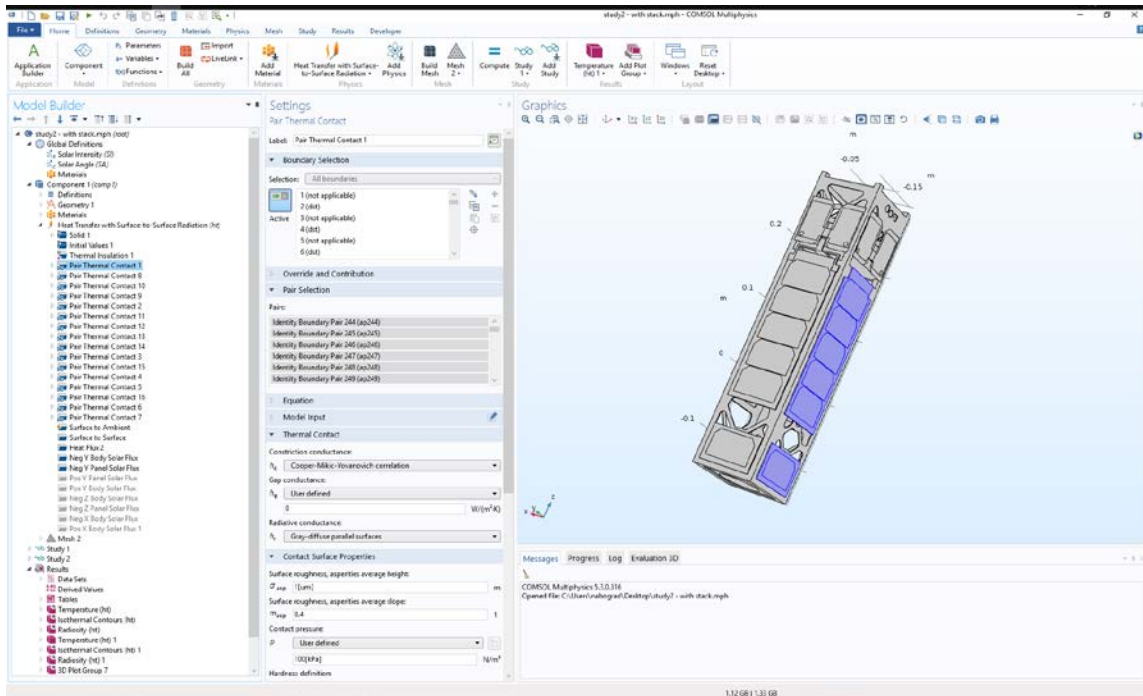
Figure 21: Pairing the thermal contacts was an important step to defining the heat transfer.

Another subtab, for Surface to Ambient radiation, was made using the Diffuse Radiation option and all of the boundaries that lied on the surface of the CubeSat were selected. These surface boundaries were selected to model the heat transfer between the surface of the CubeSat and the ambient environment and temperature which was set to the ambient space temperature of 2.7 K. Another subtab that uses the Diffuse Radiation, was Surface to Surface radiation, where all of the inside surfaces were selected.

To model the heat flux from the free molecular flow on the front of the 4U CubeSat the Heat Flux option was selected. Using the calculated heat flux from the free molecular heat transfer equations, an inward heat flux of 2.44 W/m^2 was applied to the front face of the CubeSat. The Heat Flux option was used to model the Solar Radiation, so this heat flux was also applied as a general inward heat flux. However, the equations that model these heat fluxes were split into two selections since each material has a different surface emissivity. For the selection of the chassis, connector and solar array backing, we modeled the heat flux using the Eq. (2):

$$q_0 = S\varepsilon_{Al}SI(t)\sin(\frac{\pi SA(t)}{180}) \;\; \text{Eq. (2)}$$

Similarly, the heat flux for the solar panels was modeled using the equation:

$$q_0 = S\varepsilon_{GaAs}SI(t)\sin(\frac{\pi SA(t)}{180}) \;\; \text{Eq. (3)}$$

The solar data was incorporated by creating a variable for luminosity (either 1 or 0 for any given time) and for the angle of the sun facing face of the spacecraft. This allowed the observation of the spacecraft on multiple heating and cooling cycles corresponding to multiple orbits. The thermal heat flux equation for the solar panels can be seen in Figure 22 below.
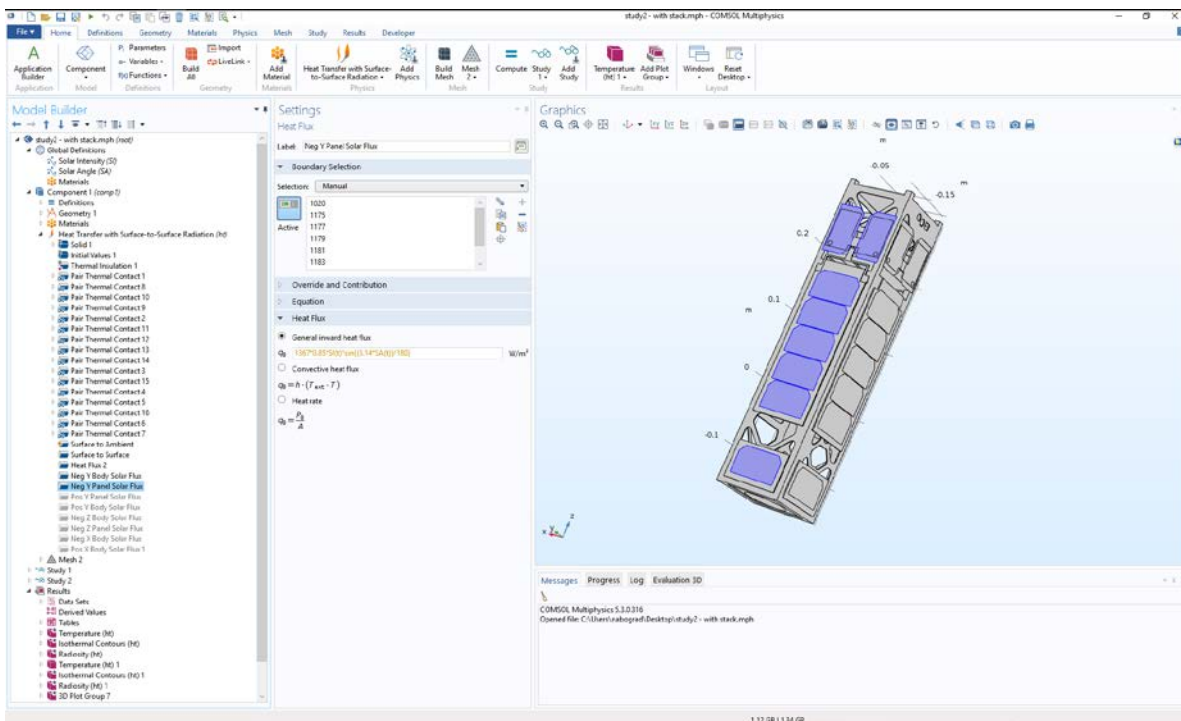
Figure 22: The thermal heat flux equation used for the solar panels.

After setting up all of the thermal physics equations, the model needed to be geometrically meshed in order for COMSOL solve them and return results. Over the course of the thermal analysis, we went through many models but continually needed to de-feature and simplify the CAD model because the mesh would either error due to the many small surfaces and circular

geometries or have to be set to a higher setting that would produce a geometric mesh with element numbers in the hundreds of thousands. When the mesh has a very high number of elements, around 300,000 elements in the CAD model, the equation solvers require an enormous computational time and memory, and in some cases could not iterate at all. The final de-featured CubeSat model has a mesh with around 10,000 elements due to the simplicity of our model and by selecting the extremely coarse mesh setting in the size tab under the Free-Tetrahedral option for Mesh selection. Additionally, a high-fidelity mesh was considered. While impractical for the time-based solution, stationary values were measured for both the high-fidelity model and the normal mesh. These values differed by less than 2 degrees, so it was determined that the normal mesh would accurately depict results. The mesh is shown in Figure 23, and the high fidelity mesh is show in Figure 24
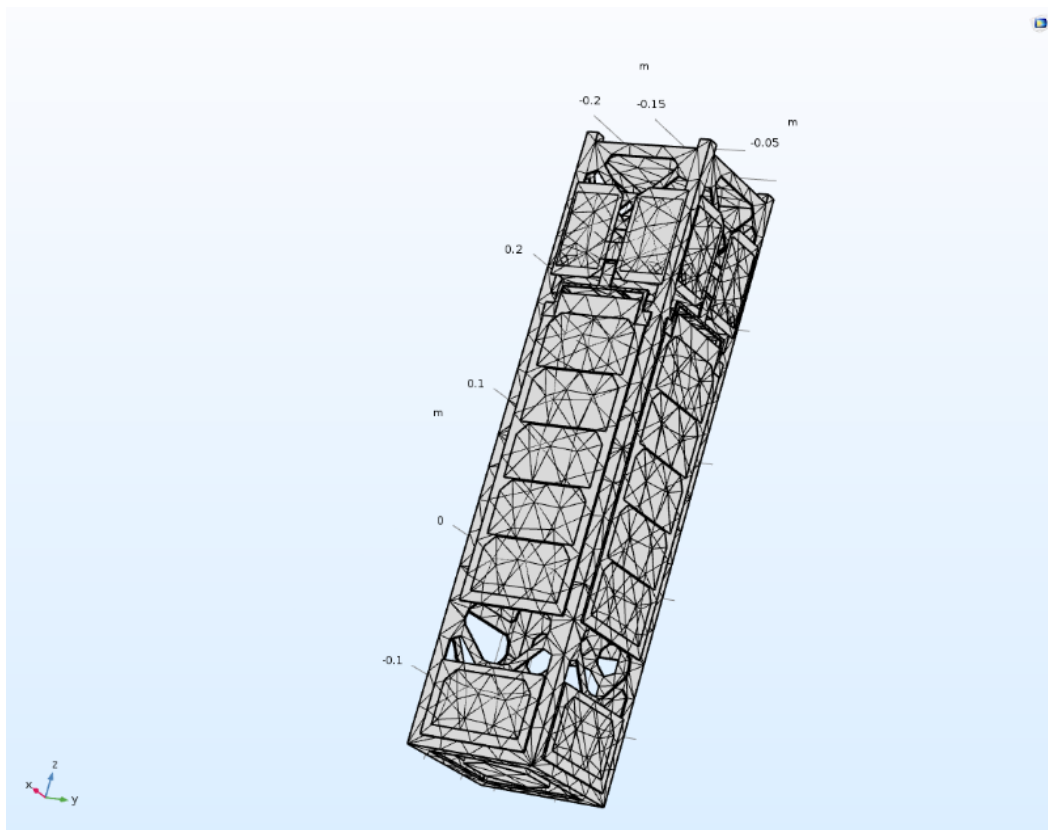
Figure 23: The de-featured 4U CubeSat model mesh.
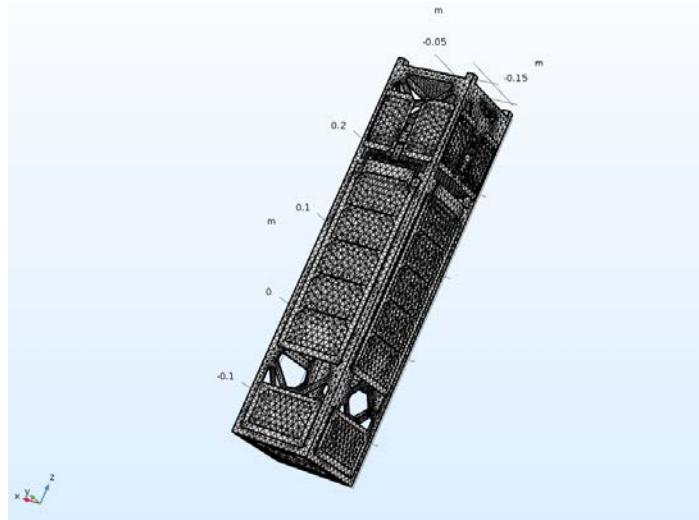
Figure 24: The de-featured 4U CubeSat high fidelity model mesh.

Two simulations were performed: an unsteady state and a steady-state. For the unsteady simulation, the time selection had to match the orbit time and time step that the STK orbital data was recorded in. The simulation was performed for 14400 seconds with a time step of 30 seconds, which is input in the "Times" box as "range (0,30,14400)". By running the simulation for this total time we were able to see multiple orbits, which incorporated the heating and cooling cycle as the 4U CubeSat passed through illumination and eclipse. The steady-state simulation assumes steady-state thermal heat fluxes. In some cases, the relative tolerance for the convergence of the solvers needed to be adjusted, however only by limited margins with a maximum of 0.03.

The COMSOL results for the thermal analysis, were exported into a GIF of the surface temperature analysis over the four hour orbit time. A video was also recorded a side of the CubeSat orbit animation from STK in conjunction with the GIF of the thermal analysis by using a screen-capturing software called Screencast-O-Matic (Screencast-O-Matic, 2018) and syncing up both animations. A screenshot of the GIF is shown below in Figure 25.
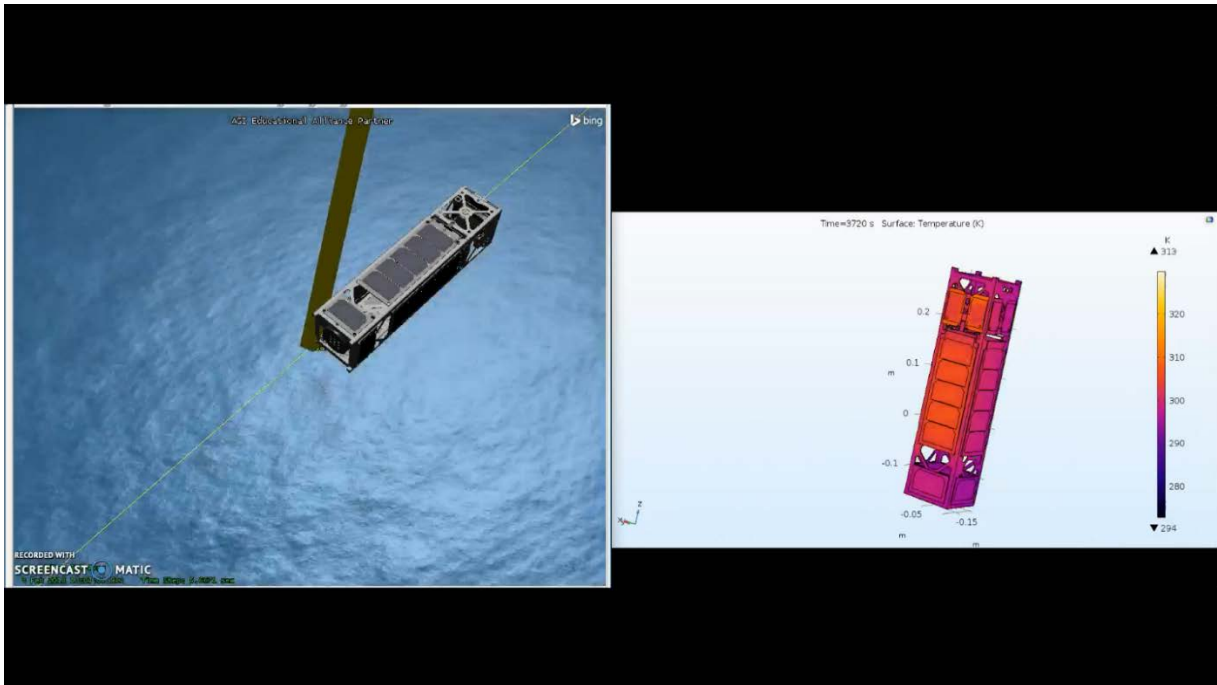
Figure 25: The use of COMSOL and STK together allowed us to see the heat change synced together.

4.1.2 Results

For the eLEO CubeSat, the heating due to atmospheric friction was considered in the simulation. We found that the largest contribution to heating was from solar radiation. The eLEO CubeSat reached a maximum temperature of 305 K and fell to a minimum temperature of 243 K over four hours. For the thermal analysis, the CubeSat begins in illumination and moves through 2.5 orbits over the course of 4 hours (See Appendix D for illumination and eclipse times). With an initial temperature of the CubeSat to 305 K and over time the CubeSat's temperature range is dropping. In Figure 26, the surface temperature of the CubeSat is shown after 60 seconds in orbit. The temperature is close to the initial temperature, ranging from a minimum of 302 K to a maximum of 305 K. The lower temperatures, shown in red-orange, are due to the solar panels overlapping their respective panel backing.
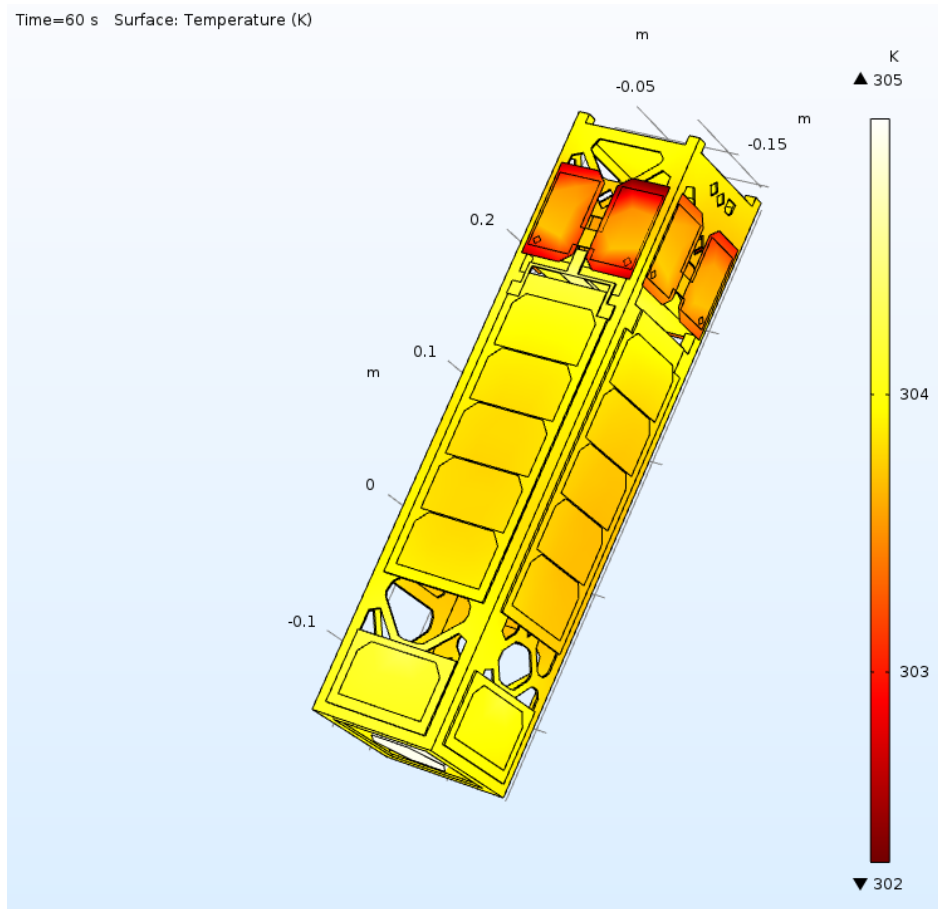
Figure 26: Surface temperature for the eLEO CubeSat after 60 seconds in orbit.

For each consecutive orbit the maximum temperature that the CubeSat reaches decreases after a period of illumination. Similarly, the minimum temperature drops after consecutive orbit periods in eclipse. A conclusion is that the temperature of the CubeSat is decreasing over time and that the time spent in illumination is not enough to heat the spacecraft to maintain tolerable temperatures. In Figure 27, the CubeSat has been in orbit for 13560 seconds (3.767 hours) and the surface temperature ranges from a minimum of 243 K to a maximum of 265 K. It is at this time, that the CubeSat reached the lowest temperature of 243 K for the four hour time period.
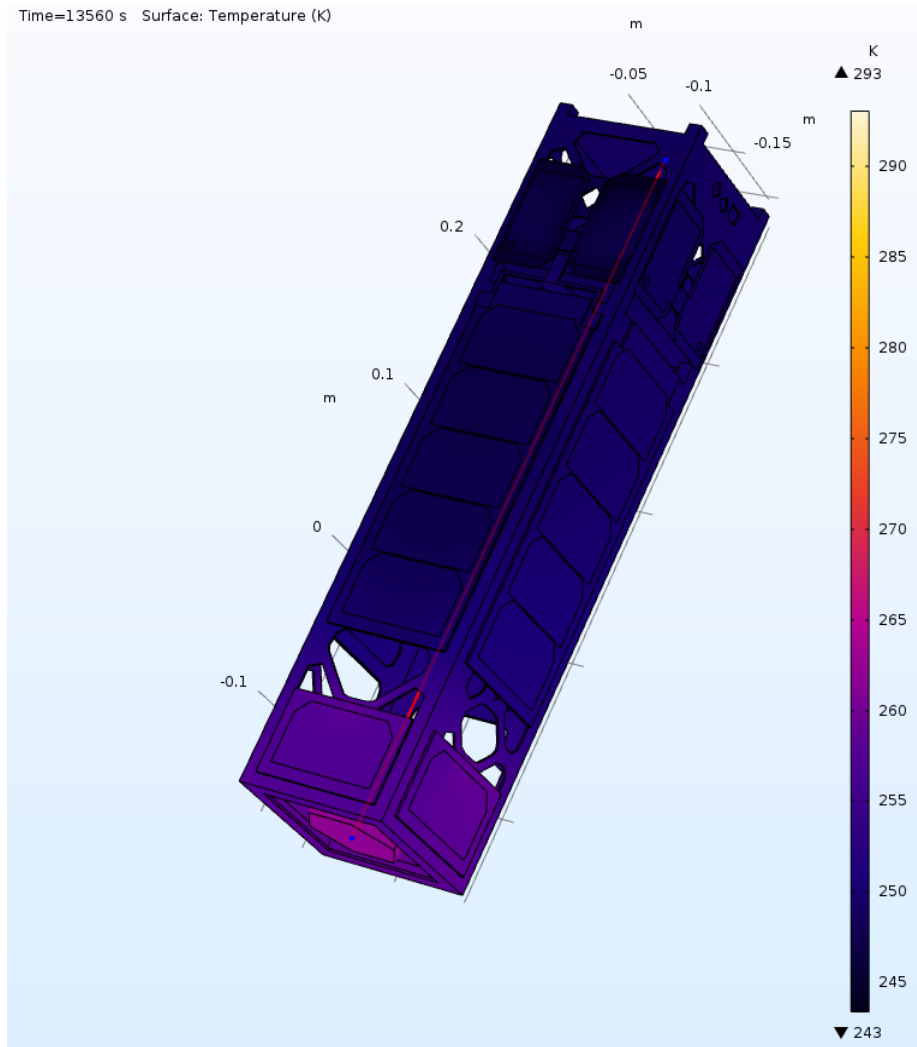
Figure 27: Surface temperature of eLEO CubeSat after 3.67 h in orbit (1).

Another run of thermal analysis was performed to try and determine the steady state temperature of the CubeSat. This run had the CubeSat orbit for one day (86400 seconds). The maximum temperature for this run was still 305 K, however the minimum temperature was 236 K, a decrease from the four hour run minimum. It is difficult to determine an exact steady state temperature, but during the final 4 orbits the CubeSat temperature stayed within in a range between 236 K in eclipse and 281 K in illumination. The Figure 28 shows the CubeSat reaching a low of 236 K at 82800 seconds (23 hours).
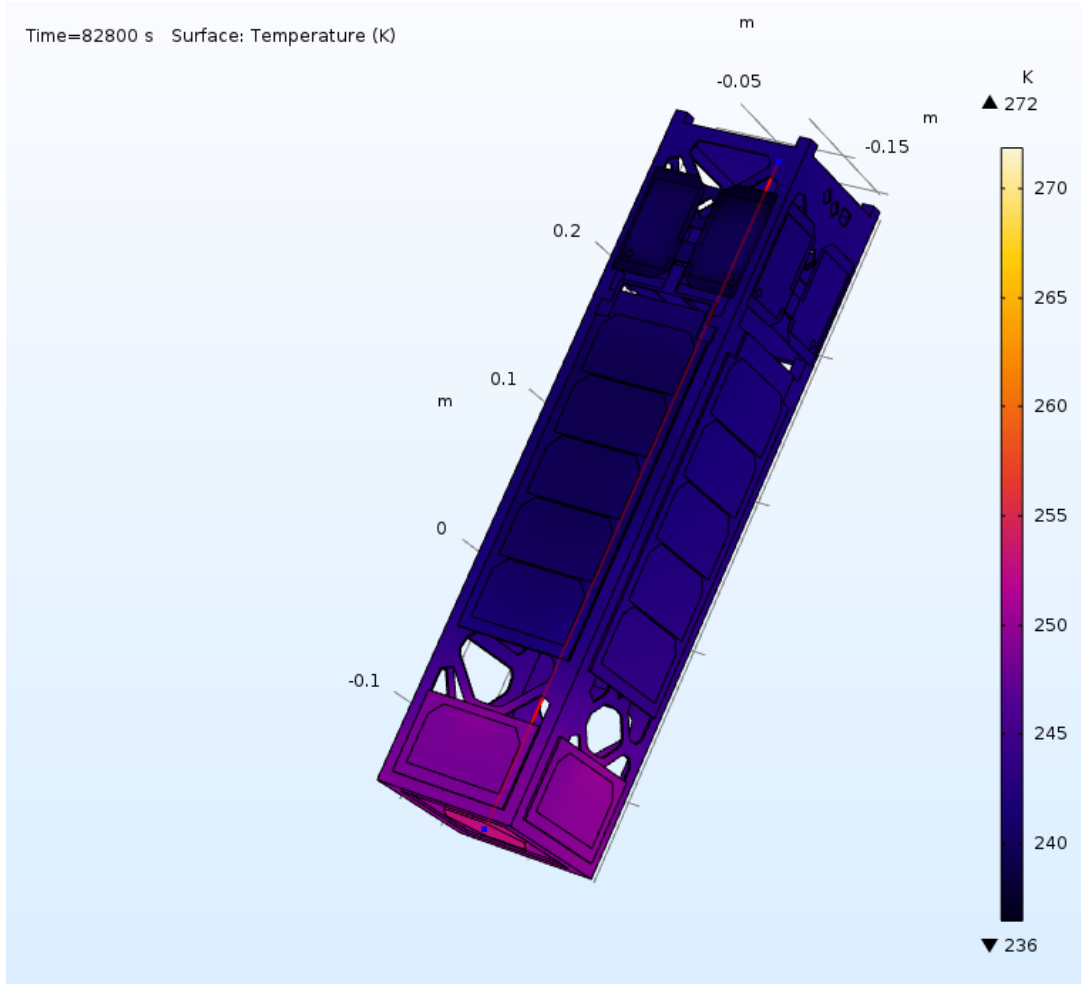
Figure 28: Minimum temperature of eLEO CubeSat at 82800 s (2).

Due to limitations within COMSOL, we believe these temperature results are too low compared to actual temperatures. COMSOL cannot apply heat fluxes to percentages of surfaces by area so that it would match where solar heat fluxes would hit the CubeSat. As a result, COMSOL cannot simulate how the sunlight and shadows change as the CubeSat orbits. To overcome this problem, the team decided to approximate this heat flux by applying the solar flux angle as a percentage to the entire surface. This means that while the analyzed faces received the "correct" amounts of heat flux, residual heat that wasn't accounted for was lost, meaning the CubeSat is actually receiving slightly less heat than it would in reality. This could be a possible explanation for why the CubeSat was becoming so cold.

The team ran another COMSOL simulation with the same time parameters that treats the solar heat flux hitting the CubeSat's surface as either total illumination or total eclipse. This simulation would be an overestimate since the angle of the sun is not being applied and therefore the CubeSat is heating up more than it would in actuality. This simulation resulted in a maximum temperature of 316 K and a minimum temperature of 265 K which is well within the operational temperature range. These are shown in Figure 29 and Figure 30

Figure 29: Maximum temperature of eLEO CubeSat without inclusion of solar angle.

Figure 30: Minimum temperature of eLEO CubeSat without inclusion of solar angle.

The operational temperature for the CubeSat chassis ranges from 233.15 K to 358.15 K. From the results of our simulations, we believe the simulation that included the solar angle resulted in a
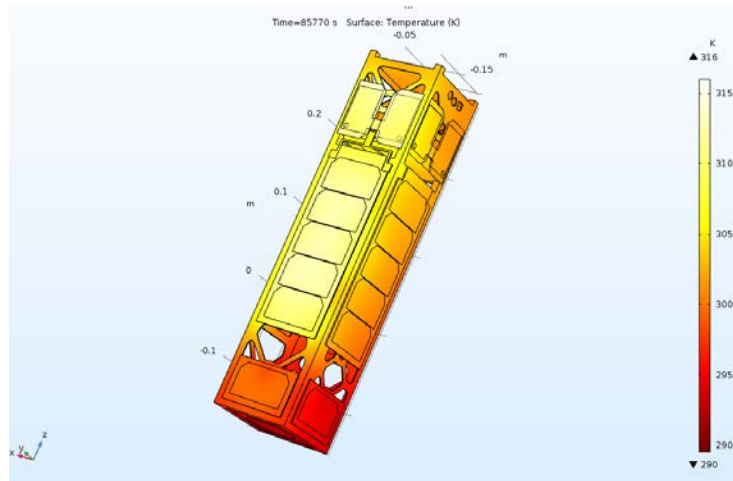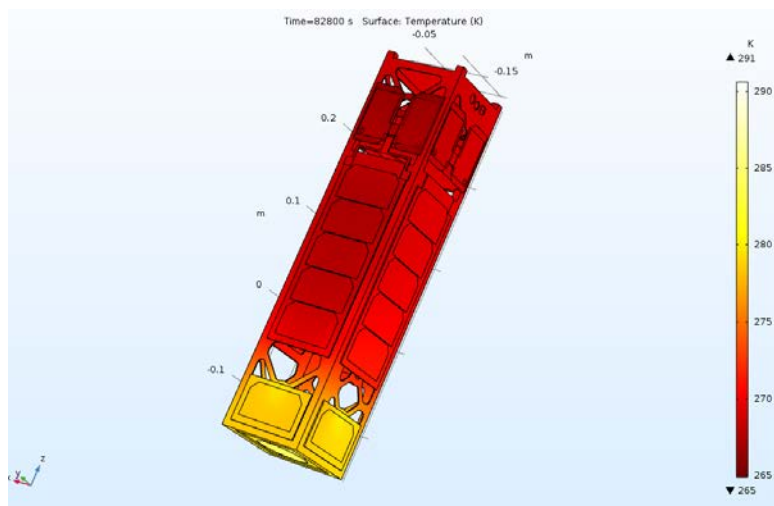
low approximation where the temperatures the CubeSat reached were just barely too low. Likewise, the simulation without incorporating the solar angle which resulted in the CubeSat being well within the operating range is most likely a slight overestimate, and the CubeSat would not reach temperatures as high. We believe that actual temperature performance will be between the high and low simulation results and that the CubeSat will remain with the operational range. Additionally the heat produced by the electronics and thrusters were not taken into account for this simulation. It is possible that this heat will keep the CubeSat warm enough for the electronics to perform. In that case, a passive cooling system could be advised, in the form of a radiative coating to reflect more incident solar radiation

4.2 LEO 16U CubeSat Thermal Analysis

In order to ensure the 16U CubeSat is within recommended operational and survival temperatures throughout its mission, thermal analysis using COMSOL was performed and a three-dimensional temperature profiles CubeSat were generated.

As with the 4U CubeSat, the main goal of the analysis is to model every component onboard the CubeSat and estimate an anticipated temperature range. Thermal control systems would then be implemented to ensure no component has an anticipated temperature range outside of its survival temperature. Thus for each component in the parts list, there is an anticipated temperature range, an operational temperature range, and a survival temperature range. Anticipated is the result of the analysis, operational is the manufacturers' recommended temperature range for ideal operation, and survival is the range in which the component does not suffer permanent damage.

4.2.1 Approach

The thermal analysis process can be broken down into four phases. The first phase is evaluation of the heat fluxes. For the LEO mission there are three major sources of heat: solar radiation, the

earth's blackbody radiation, and albedo flux. Solar radiation is the energy coming from the sun and affects the illuminated portions of the CubeSat. Earth's blackbody radiation is the radiation caused by the heat of earth and effects by the portion of the CubeSat facing the earth. Albedo flux is the reflected sunlight off of earth's surface and, like the blackbody radiation, is felt by the portion facing the earth.

The second phase is the generation of a de-featured CAD model. This model has every component included to scale however, many of the components in the 16U CubeSat are necessarily de-featured in order to reduce the computational requirements of the COMSOL simulation. The de-featured CAD model needs to accurately reflect size, material, surface areas and thermal contacts.

The third phase is to set up the simulation in COMSOL. This includes setting the initial temperature, inputting the heat sources, heat loss sources, and materials. This phase is highly iterative and may require many simulations to produce an accurate result.

The final phase is thermal control implementation. Once the first simulation has been run, the anticipated temperatures for each component should be compared to the survival and operational ranges for each. If any anticipated temperature is outside of the operational or survival limit, thermal control measures must be taken. For the purposes of this mission the thermal control measure is the surface emissivity of exterior faces. This emissivity value changes how much heat is radiated away from the surface and can be controlled using a wide variety of paints, coatings or other coverings.

4.2.1.1 Data Collection

STK was used for most of the data collection in this section. Specifically, it was used to determine the spacecraft-sun vector for every time step in the orbit. This vector will be decomposed

to produce the illumination and heat flux on each face of the CubeSat. For blackbody radiation from earth, and albedo flux analytic approximations were used.

4.2.1.2 Solar Radiation

The most influential heat source is solar radiation. Since the CubeSat for the LEO mission is not sun-synchronous there will be six heat fluxes, one for each face of the CubeSat. In order to calculate these six heat fluxes some assumptions were made about the orientation of the CubeSat in flight. First the CubeSat assumed to be orbiting with the Z axis aligned with the velocity vector as shown in Figure 31. Second, the CubeSat's negative X axis is assumed to be aligned with the nadir vector, as seen in Figure 31. These assumptions together also mean that there is no rotation about the Z axis.
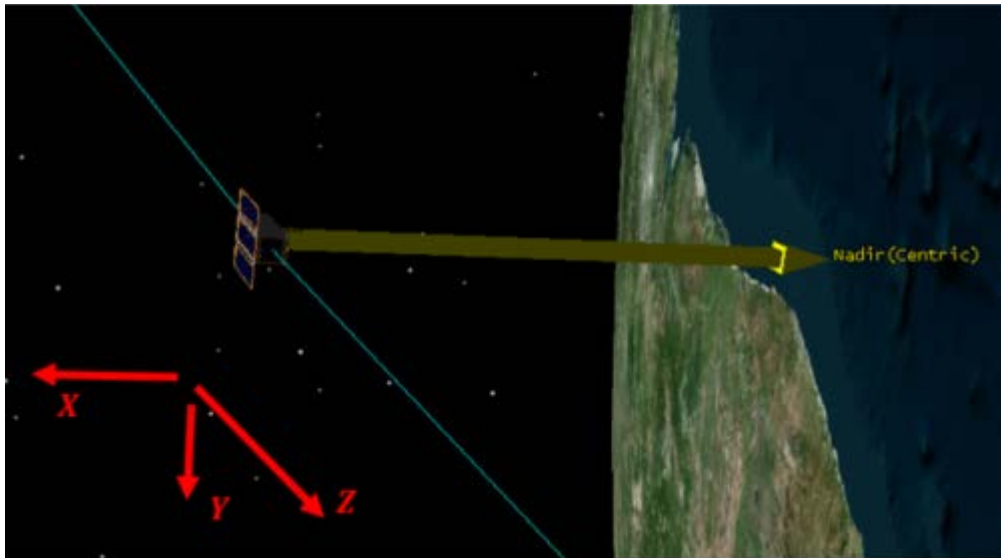
Figure 31: The 16U CubeSat orientation.

To obtain values for the heat fluxes an attitude sphere was used. This attitude sphere is a coordinate system using two angles to represent every point on a sphere. The sphere is centered on the CubeSat and the sun vector is represented in terms of these two angles. The attitude sphere is shown in Figure 32.
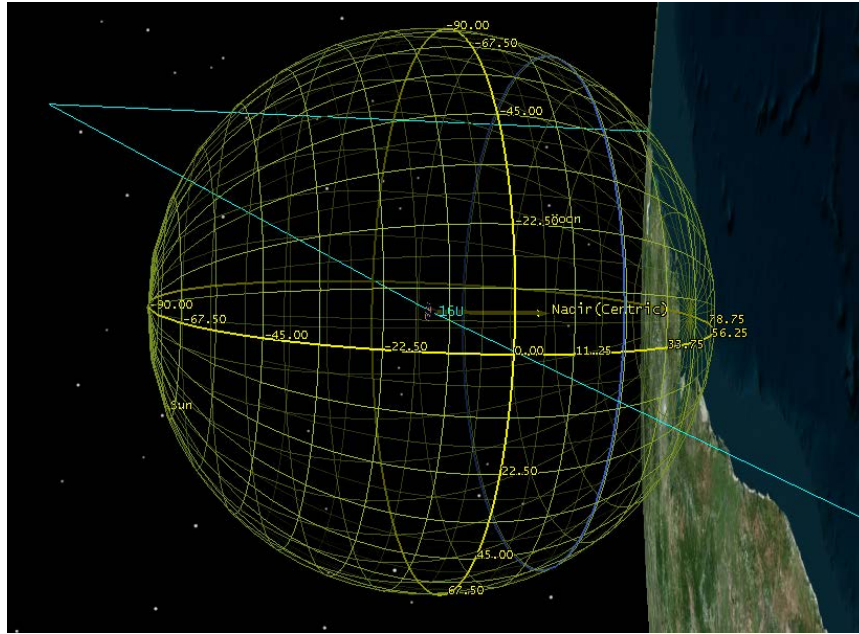
Figure 32: The attitude sphere used in the evaluation of heat fluxes.

For consistency, we will call these attitude sphere angles theta and phi as seen in Figure 33.
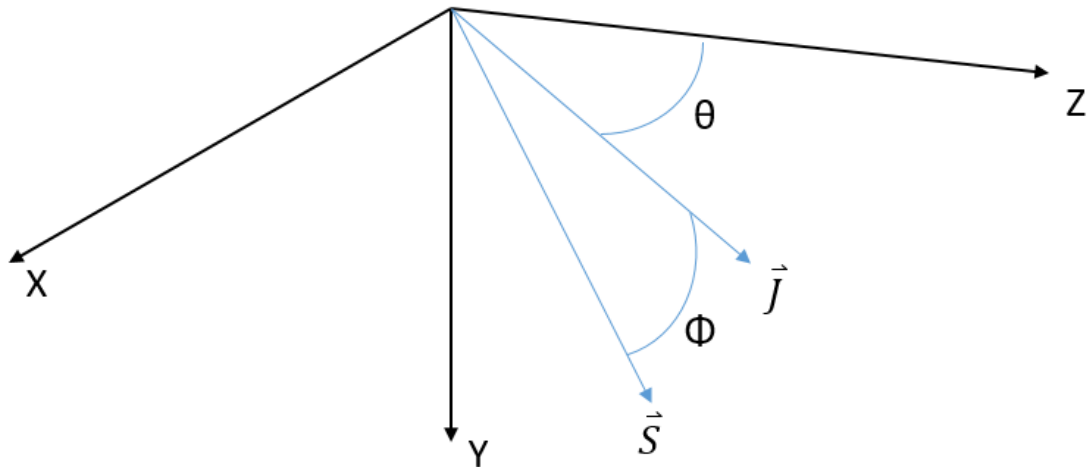
Figure 33: The attitude sphere angles.

Theta is measured from Z to J in the X-Z plane and Phi is measured from J to S in the J-Y plane. Here J is an arbitrary vector being used to evaluate theta and phi, and S is the sun vector. To calculate the heat flux on each face, the following equation was used.

$$Hs = S * A * \cos(b) \qquad \text{Eq. (4)}$$

Where Hs is the heat rate in watts, S is the solar irradiance at earth in watts per square meter, A is the area of the surface and b is the angle between the sun vector and the face normal. The difficult part of this equation is calculating b for each time step. The method for calculating b is shown in Figure 34.
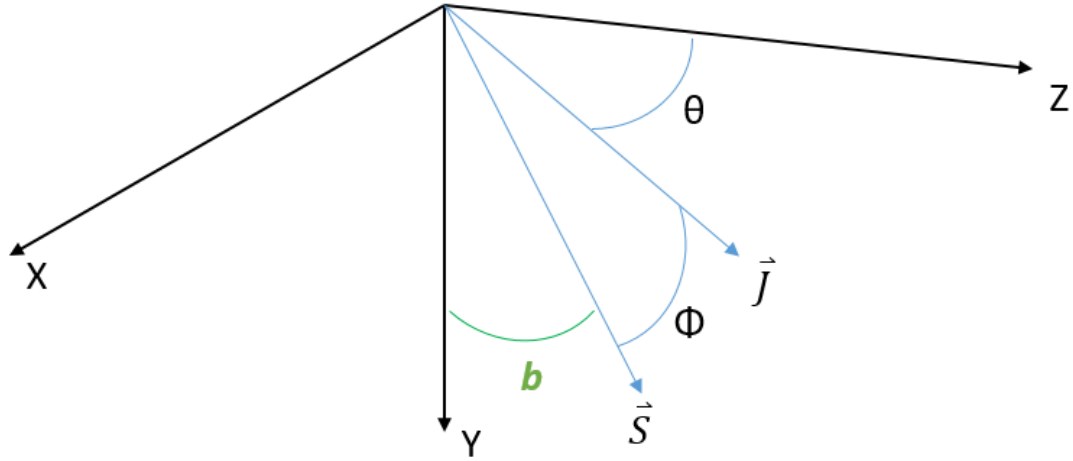
Figure 34: The utilized method for calculation of the angle (b).

$$b = \text{acos}(\vec{S} \cdot \vec{N}) \qquad \text{Eq. (5)}$$

$$\vec{S} = \begin{bmatrix} \sin(\theta) \cdot \cos(\phi) \\ \sin(\phi) \\ \cos(\theta) \cdot \cos(\phi) \end{bmatrix} \qquad \text{Eq. (6)}$$

The $\vec{N}$ vector in Figure 31 represents the normal vector of a face. $\vec{S}$ and $\vec{N}$ are both unit vectors and for the figure above $\vec{N}$ is the positive Y normal vector from Table 6. The six face normal vectors are listed in Table 6. Any time the angle b is greater than ninety degrees the heat flux on that face is reduced to zero since a b value greater than ninety indicates that the face is not illuminated.

Table 6: Normal Face Vectors

Face	Normal Vector
Positive X	(1,0,0)
Negative X	(-1,0,0)
Positive Y	(0,1,0)
Negative Y	(0,-1,0)
Positive Z	(0,0,1)
Negative Z	(0,0,-1)

4.2.1.3 Blackbody Radiation

Earth's blackbody radiation is easier to calculate than the solar radiation and is given following Wertz (1999):

$$Hb = K * A * \left(\frac{Re^2}{Re^2 + h^2} \right) \quad \text{Eq. (7)}$$

Where K is the blackbody radiation at earth's surface, approximately 231 watts per square meter, A is the area of the surface, Re is the radius of earth, and h is the altitude of the spacecraft. For this mission, h is 500 kilometers and the heat flux is assumed to be through the nadir aligned face only, thus blackbody radiation will be constant over the mission.

4.2.1.4 Albedo Flux

Albedo flux is the heat from the sunlight being reflected off of earth's surface following Wertz (1999).

$$Ha = a * S * F * A \quad \text{Eq. (8)}$$

In the above equation here, Ha is the albedo heat rate in watts, a is a constant of reflectivity, (approximately 0.35 for earth), S is solar irradiance at earth, (approximately 1361 watts per square meter), F is the fraction of sunlit earth visible, and A is the area of the surface. The albedo flux is assumed to be through the nadir aligned face only.

Albedo flux is a function of the spacecraft's field of view (FOV). In the above equation only F the fraction of sunlit earth, is changing with time. To calculate this F we need to know the field of view of the CubeSat given by Wertz (1999) as:

$$\sin(FOV) = (\frac{Re}{Re+h}) \qquad \text{Eq. (9)}$$

FOV is the angle between the points directly below the spacecraft on earth, to the visible horizon of earth. Twice this value is the full angle visible from the spacecraft. For the LEO mission the FOV is approximately 68 degrees.

In order to approximate Ha the following equation was used, its values at certain points on the orbit are shown in Figure 35.

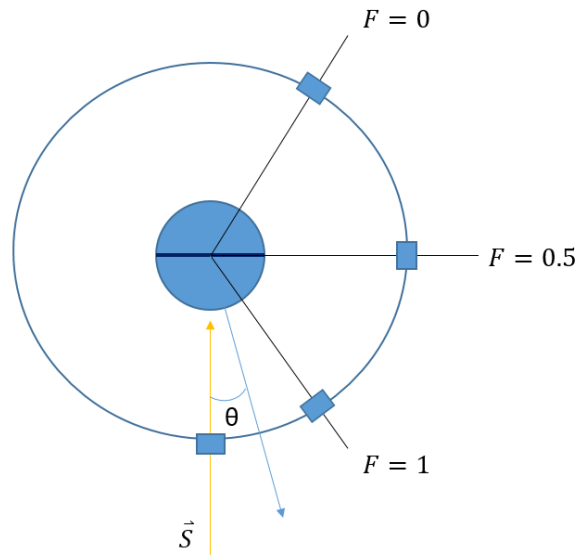$$F = 1 - \frac{\theta-22}{136} \qquad Eq.\ (10)$$

Figure 35: The fraction of sunlit earth visible.

Generally speaking however, the fraction of sunlit earth has a value of one when the earth, CubeSat and Sun are roughly collinear, zero when the CubeSat is in shadow behind earth, and a fractional value in between. The fractional values are not perfect, but function based on the

assumption that the sun illuminates roughly half of earth at a time. The value of F then, is 0.5 when the CubeSat is directly above the divide from illuminated to shadow. Given the assumed orientation for thermal analysis, the flux from albedo was assumed to be through the nadir aligned face only.

4.2.1.5 De-featured CAD Model

In order to limit simulation time in COMSOL, a simplified model of the 16U CubeSat was created. This model turns the circuit stack components into solid cubes. This is due to the high complexity in the CAD models provided by retailers. These models simply contain too many boundaries which COMSOL would attempt to include in the calculation. This would cause the calculation time to spike by an order of magnitude.

In order to retain a similar profile for heat transfer, the connection points for the model were retained. These connection points are the support structures holding the circuit stack to the CubeSat frame and by keeping these connections the heat properly transfers to the simplified circuit stacks.

The remaining components were kept as close to the original design as possible. A step by step assembly of the simplified model is in Appendix E.

4.2.2.5 COMSOL Simulation

Table 7 provides the options used in COMSOL to perform the thermal analysis.

Table 7: Options selected for COMSOL 16U CubeSat simulation.

Variable	Value
Space Dimension	3D
Physics	Heat Transfer in Solids
Study	Time Dependent
Result	Surface Temperature

The model was imported and the option form union was selected, as this option helps to define what surfaces are in contact. The model used was covered in depth in Appendix E, and the version imported to COMSOL can be seen in Figure 36. The components of the model, apart from the solar panels, were defined as aluminum. The specific type and values for this material are in Table 11.
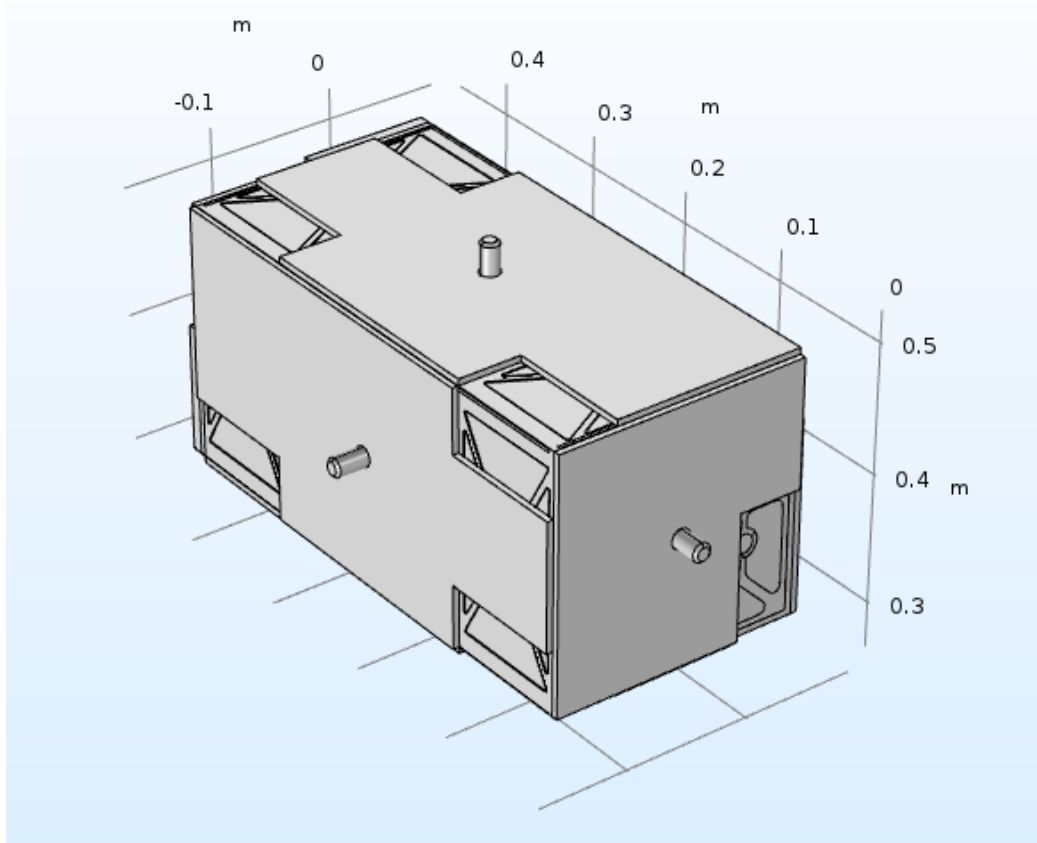

Figure 36: The de-featured CAD model for the 16U CubeSat.

The boundary conditions applied to the model are shown in Table 8. The purpose of each will then be discussed individually.

Table 8: COMSOL boundary conditions used in the 16U CubeSat simulation.

Boundary Condition
Heat Flux
Diffuse Surface
Open Boundary
Thermal Contact

The heat fluxes from data collection were applied to the whole of each face, including the thruster. The thrusters would not receive quite as much heat as the model assumes, but this quantity of heat has a negligible effect on the rest of the simulation. The area selected for a single heat flux is shown in Figure 37. This is only one of the six heat fluxes applied, one to each face of the CubeSat.
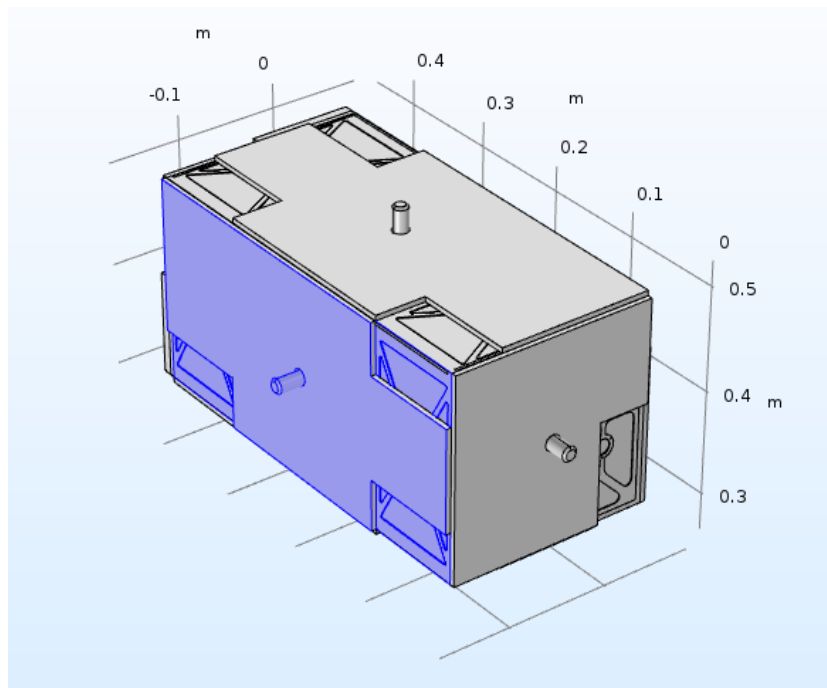
Figure 37: The heat flux applied per face on the 16U CubeSat.

In addition to these heat fluxes, the exterior of the CubeSat was modelled as a diffuse surface. Two sets of boundary conditions were used, one for the metal exterior, and one for the solar panels. This allows separate emissivity values to be assigned to each, the purpose of these values is discussed in the thermal control section.

The diffuse surfaces, seen in Figure 38, were made to radiate heat to an ambient temperature of 2.7 Kelvin, the approximate temperature of space. Together, these surfaces are the main means of heat loss.
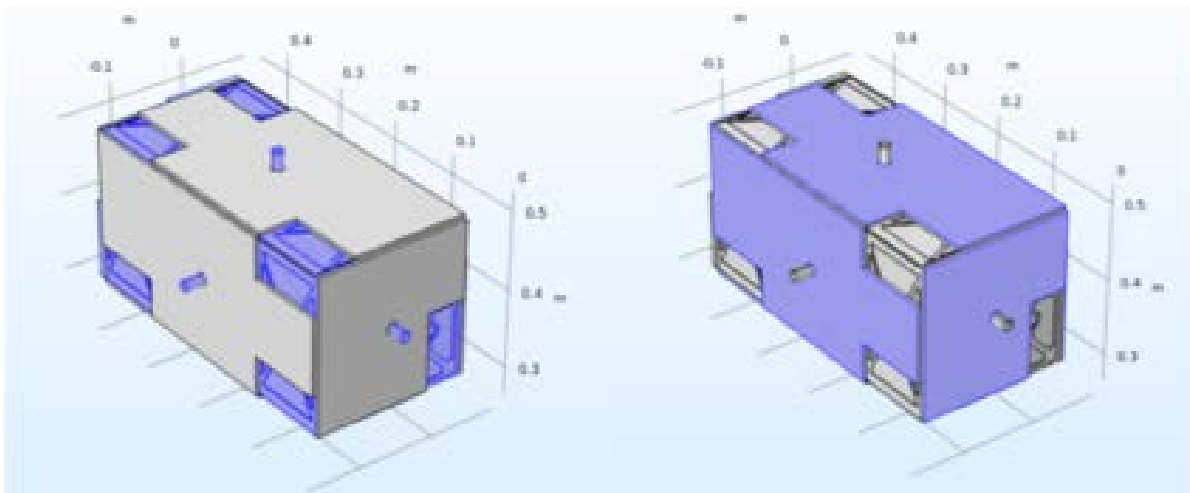
Figure 38: The COMSOL boundaries selected for the 16U CubeSat.

The entirety of the interior of the model was subject to the open boundary condition. This allows heat transfer across open spaces via conduction convection and radiation, however since no ambient material was defined only radiative heat transfer is simulated. This option also models any non-defined exterior boundary as an open boundary as well, filling in any missed faces in the diffuse surface boundaries.
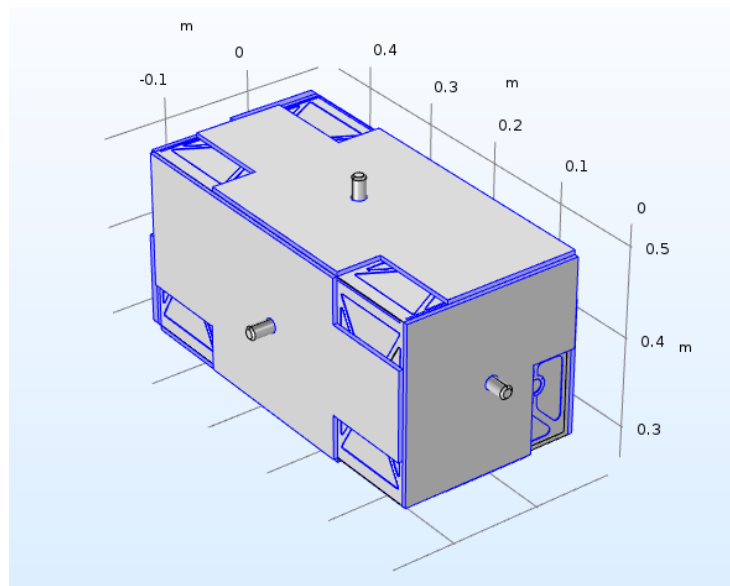
Figure 39: The thermal contact boundaries selected for the 16U CubeSat.

Thermal contact was applied to the whole model, as seen in Figure 39, and because the geometry was imported as a union, COMSOL is able to automatically determine what surfaces are and are not in contact. This option prevents hot or cold points from occurring during simulation and ensures that heat is being properly transferred throughout the entire model.

4.2.1.6 Mesh Model

The mesh used for the simulation was a COMSOL predefined size. Coarser was chosen because it allowed simulations to be run quickly and accurately. The mesh is shown in Figure 40. In order to ensure that the results were not a function of mesh geometry a higher fidelity model using COMSOL predefined size fine was simulated shown in Figure 41. The coarser model had 528,000 elements, and the fine model had 877,000 elements.
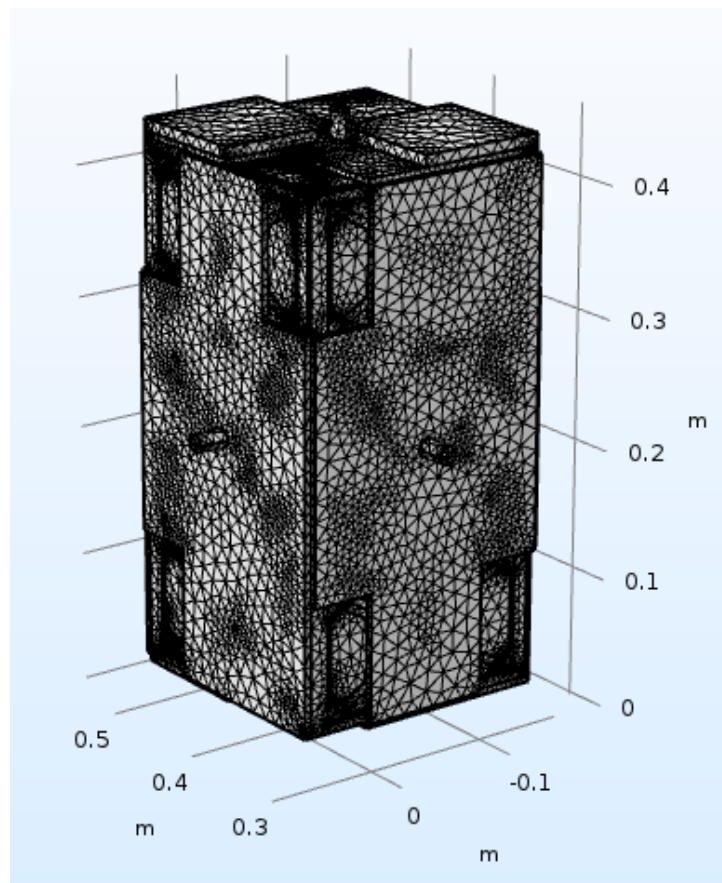
Figure 40: The 16U CubeSat mesh shown with the coarse setting.

71
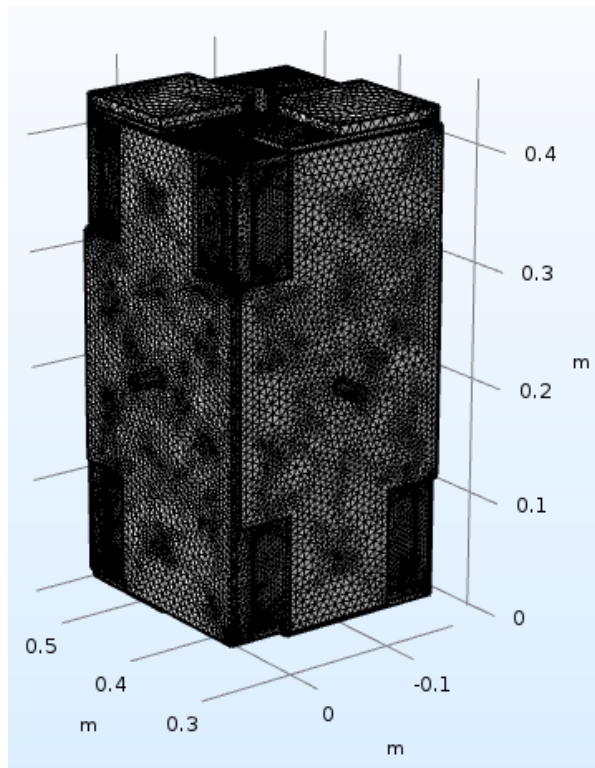
Figure 41: The 16U CubeSat 6U mesh (Fine).

The comparison of the results from these two simulations can be seen in the results section. The high and low temperature graphs are nearly identical.

4.2.1.7 Thermal Control

Passive thermal control was used to retain the components within acceptable operating conditions. This passive control consisted of an emissive coating for select surfaces, and careful consideration of solar panel choice. Since the only real method for dispersal of excess heat energy in orbit is radiation, the higher the emissivity's chosen for the coating and solar panels, the more energy these two surfaces radiate away while in shadow. The surface coating baseline was based on the analysis of previous WPI CubeSats. In JB1701, the baseline emissivity was 0.55. This is achievable using a number of thermal paints, coatings or materials. This baseline emissivity corresponds to aluminum paint (Mikron), but with proper material choice many other emissivity's can be used. The emissivity of the solar panels functions slightly differently. Many papers have

been written about the subject and findings show that specific designs vary the emissivity, but NASA specification sheets indicate that most are in the range of 0.75-0.85, additionally, more recent papers place the highest emissivity at 0.9 (Zhu et al, 2014).

The final two sections are iterative. This means that the simulation was run, the expected thermal loads identified at the hottest and coldest points, and then tabulated versus the operating and survival temperatures for each component. If any component deviates from its survival range, or multiple components deviate from operational range then the simulation is run again with new emissivity values. Since the emissivity can be an independent variable all that is needed is to ensure that there is a space-rated material available with the desired emissivity.

4.2.2 Results

With set emissivity values of 0.55 for exposed surfaces and 0.9 for solar panels every component remains within operational tolerances. Some components approach operational limits when subject to the heat loads of the polar orbit. However, this orbit was specifically selected as an upper boundary for expected heat loads. The CubeSat on this orbit is never in eclipse, meaning that it is subject to constant strong heat fluxes. This results in a higher equilibrium temperature than the other two orbits and as such the highest anticipated temperatures for the components all come from this orbit. The low temperature ranges are split between the 45 and equatorial orbit. Thus no form of active thermal control is needed to keep the components within the desired ranges.

The results of the heat analysis for the three orbits are as follows. The three orbits will be referred to henceforth as equatorial, polar and 45, due to the nature of their inclinations.

The CubeSat was modelled through five orbits to determine whether temperature trended up, down or remained roughly the same over multiple orbits. A positive trend indicated a need for higher emissivity surfaces, a negative trend indicated a need for lower emissivity surfaces, with

small fluctuations being ideal. Figure 42, Figure 43, and Figure 44 show the heat rates applied to the faces of the CubeSat for each orbit. The charts are in terms of true anomaly along orbital path, each degree of true anomaly equates to 16.08 seconds. The orbits start with a theta angle equal to 90 degrees, refer to Figure 33 of the thermal analysis chapter. The initial phi angle varied between the three orbits. Note that for these charts small fluctuations, less than 5 degrees, in the angle between the sun and normal vector for each face were simplified to constant average values.
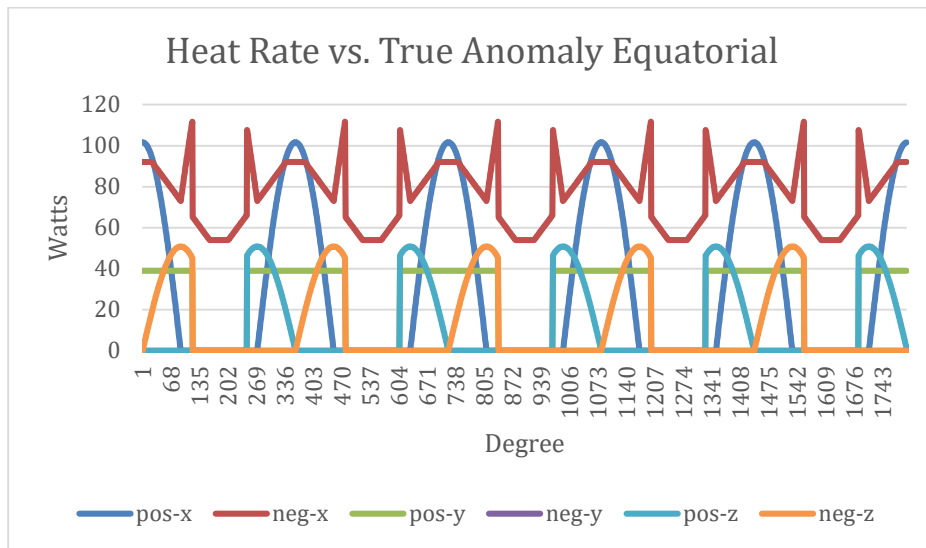
Figure 42: Heat rate vs true anomaly for an equatorial orbit.
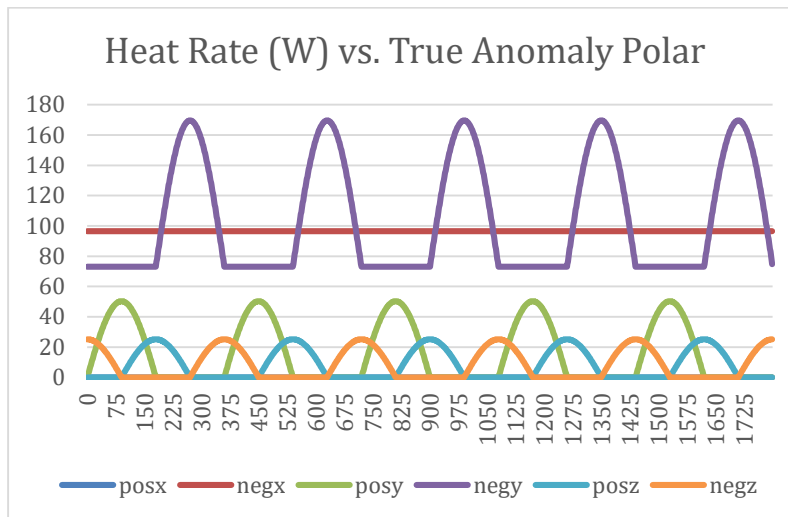
Figure 43: Heat rate vs true anomaly polar orbit.
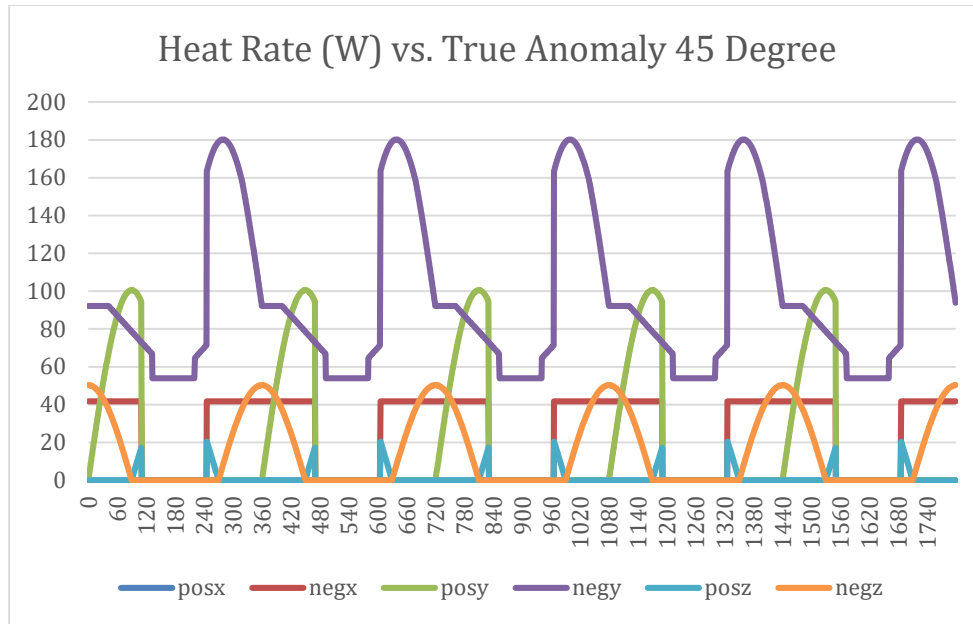
Figure 44: Heat Rate vs true anomaly for a 45 degree orbit.

The COMSOL simulations of the five orbits calculated the temperature every one-thousand seconds and were run over a range of 29000 seconds, for 29 data points each for the equatorial, 45, and polar orbits. Figure 45, Figure 46, Figure 47 and Figure 48 show the highest and lowest temperature on the 16U CubeSat for each of the orbits from these data points. The high-fidelity mesh results show the dependence on mesh geometry, given the similarity of the two plots the team concluded that the mesh size used for the simulations was sufficient.
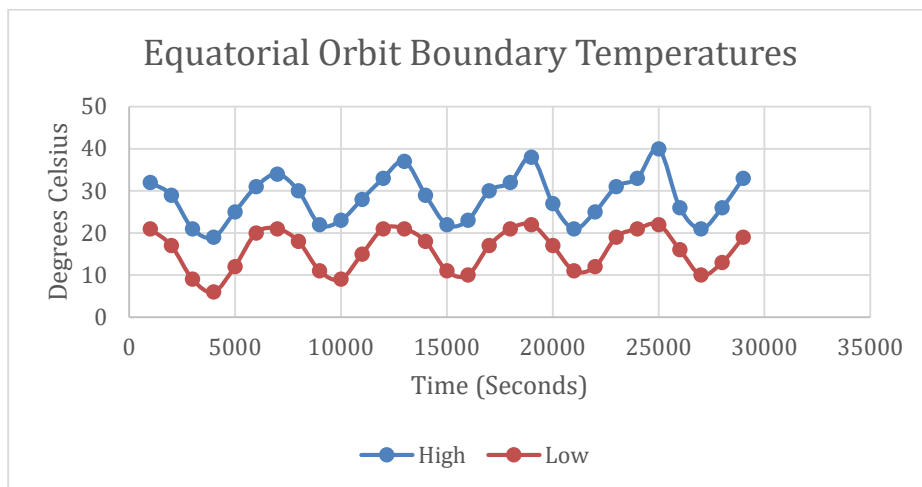
Figure 45: Maximum and minimum temperature of a 16U CubeSat in equatorial orbit.
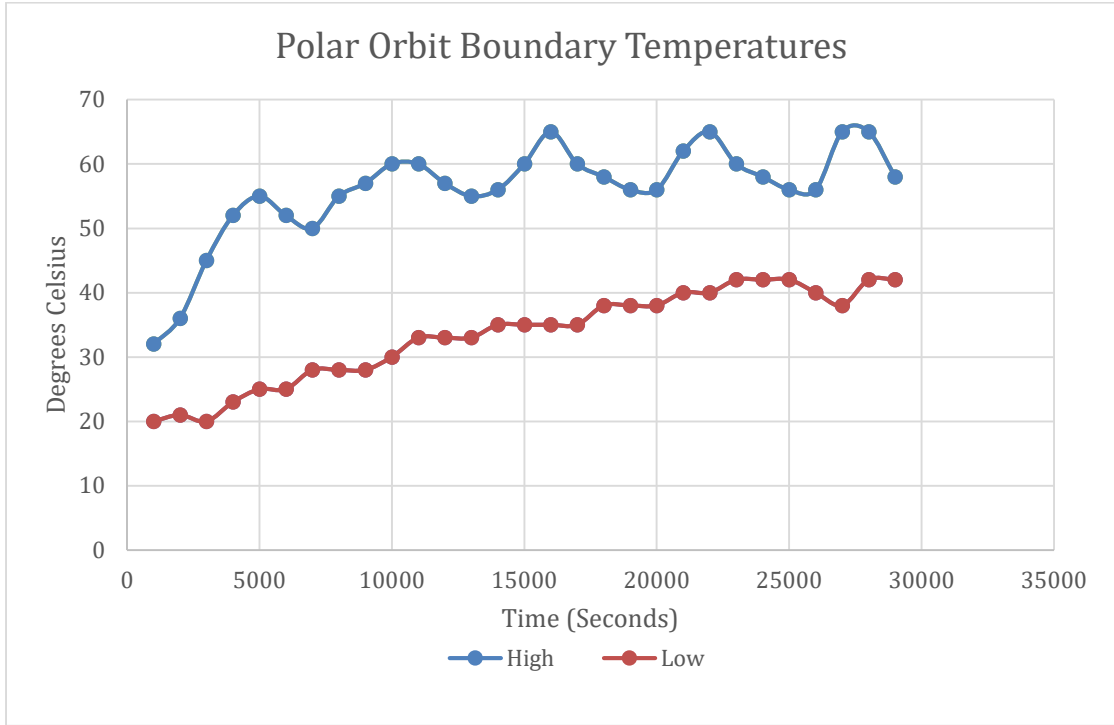
Figure 46: Maximum and minimum temperature of a 16U CubeSat in a polar orbit.
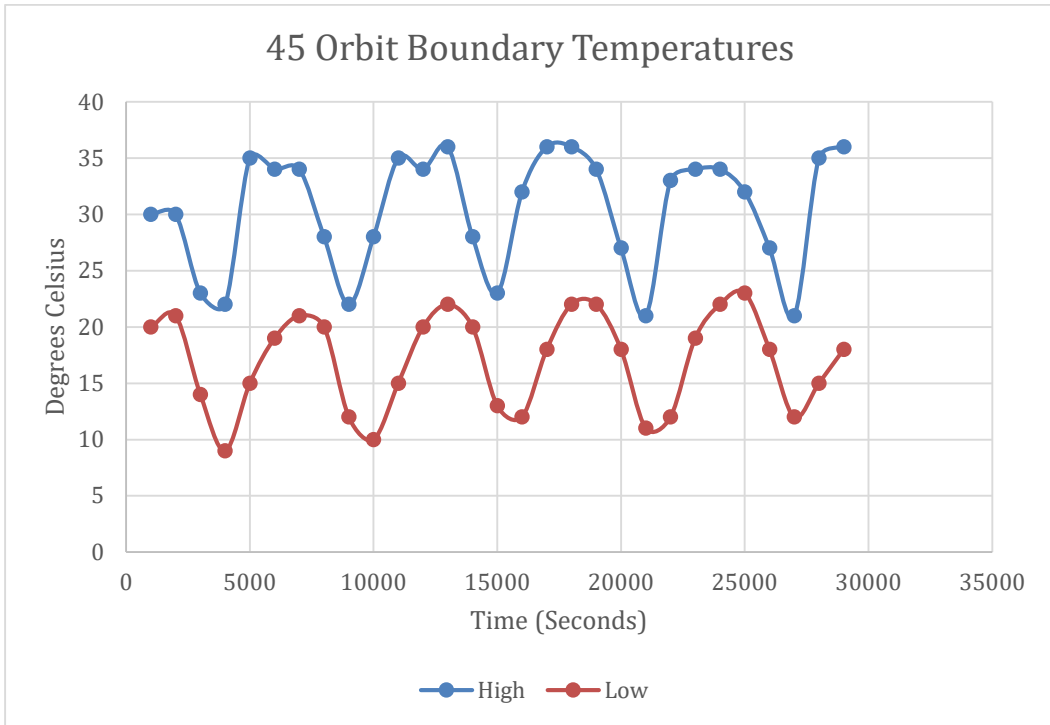
Figure 47: Maximum and minimum temperature of a 16U CubeSat in a 45 degree inclined orbit.
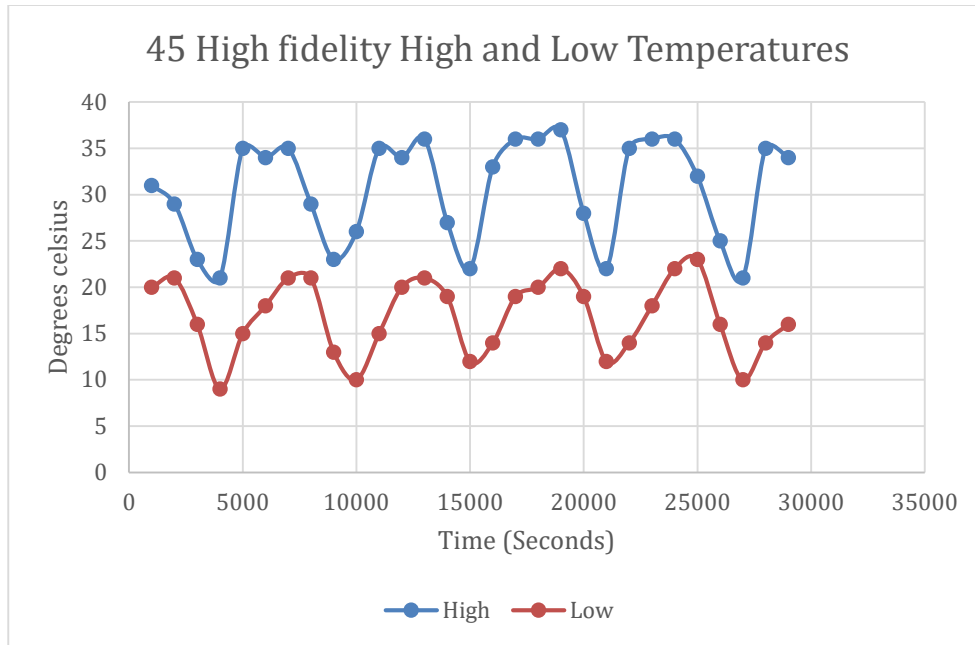
Figure 48: Maximum and minimum temperature of a 16U CubeSat in a 45 degree inclined orbit.

Operational, survival, and anticipated temperature ranges for each orbit are recorded in Table 9. Note the operational and survival ranges of some of the commercially available components were not provided by retailers. In these cases, the survival range was assumed to be from -45 degrees Celsius to 85 degrees Celsius, which is the typical range of space rated components. The items that make up the circuit stack were bundled and the smallest operating temperature range of the bundled components used.

Table 9: Electrical component expected temperature vs. normal operation and survival temperature range for the 16U CubeSat

Part Name	Expected Temp. (C)	Operating Temp. (C)	Survival Temp. (C)
Frame	[-10,70]	[-45,85]	[-45,85]
Circuit Stack	[10,50]	[-40,60]	[-45,85]
GPS	[10, 50]	[-20,50]	[-45,85]
Magnetometer	[35,50]	[-25,70]	[-45,85]
PPT	[10,70]	[-20,350]	[-45,400]
Sun Sensor	[0, 65]	[-40,93]	[-45,100]
Antenna	[25,60]	[-30,70]	[-45,85]
Solar Panels	[20, 65]	[-40,125]	[-45,140]

5 Induced Magnetic Field Analysis and Assessment of Possible Interference

In this chapter we present analysis of magnetic fields produced by the magnetic torques considered as alternatives to the PPTs onboard the eLEO and LEO CubeSats. The analysis is performed using COMSOL and provides estimates of the induced magnetic field at locations where the magnetometers onboard the CubeSats are positioned.

5.1 Introduction

Magnetic torquers have been considered as an alternative to using PPT's for attitude determination and control of both the 4U eLEO and the 16U LEO CubeSat. They produce a torque by creating a magnetic field that interacts with Earth's magnetic field. In order to determine the CubeSat's orientation both eLEO and LEO missions utilized a magnetometer, which measures the strength and direction of the Earth's magnetic field. Field lines stay in a relatively constant direction relative to the spacecraft; the orientation of the spacecraft relative to the field can then be determined (NASA JPL, 2017).

Issues arise when instruments onboard create or interfere with magnetic fields. The induced magnetic fields produced by onboard circuitry and electronics is generally negligible due to the low current running through wires. Control systems that would generally be used on CubeSats such as PPTs or magnetorquers tend to produce strong magnetic fields. If these magnetic fields produced are greater than the tolerances of the Magnetometer, the measurements of the Earth's magnetic field can be lost in the noise and indistinguishable. Magnetorquers use induced magnetic fields to produce a torque on the CubeSat and rotate the body about an axis.

A magnetic field interference study was performed by the previous Sphinx-NG MQP (NAG-1701) but did not take into account the geometry of the CubeSat, or the interference possibly produced by circuit stack. The geometry of the CubeSat was considered of negligible importance as the body

was made of aluminum, which reacts very little with magnetic fields. The circuit stack was considered too complex to model in a meaningful way. They found that magnetometers would produce a noticeable interference, but that this interference was well within the measurable bounds of the magnetometer. Their recommendations were to measure the field produced by the magnetometer and take this into account via the control system in order to determine the corrected vector for the Earth's magnetic field.

5.2 eLEO 4U CubeSat Magnetic Field Analysis

The 4U CubeSat analysis was performed following the Sphinx-NG MQP (NAG-1701) approach, but also taking into account the CubeSat chassis as well as modeling the circuit stack to a reasonable degree. This approach allowed the team to view the complex interactions of the magnetic fields produced by the three magnetorquers within the chassis and the circuit stack. To model the 4U, a steady-state simulation was set up in the COMSOL Multiphysics Electric/Magnetic Field (no currents) module to calculate the magnetic fields induced by the magnetorquers which would be operating during the detumble period for the 4U if magnetic torquers were used. First, a single magnetorquer was simulated in isolation, and the results compared to those of the Sphinx-NG MQP. This step was used to determine the accuracy of the magnetic simulation relative to the previously established work of the Sphinx-NG team. According to the magnetorquer specifications, the magnetic field produced is 47,515 milli-Teslas about the long axis of the torquer.

Then the de-featured CAD model used in the thermal analysis was utilized. The models for the magnetorquers used in NAG1701 were inserted into the model in an orthogonal orientation to each other near the center of mass as shown in Figure 49.
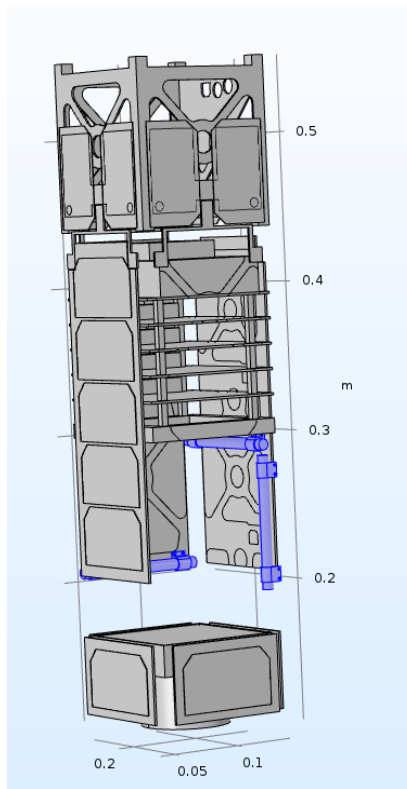
Figure 49: The possible position of magnetorquers in the 4U CubeSat.

The materials of all domains in the model were then defined. The chassis was set to be aluminum. The circuit stack is a complex mix of electronics and aluminum, and this was approximated to FR4 circuit board material. The three magnetorquers were arranged and assigned magnetic fields in the appropriate directions, along their long axes. The results re-plotted on a slice plot and the magnetic field lines are plotted in Figure 50 within the CubeSat frame. The slice plot allows the user to select a point along the slice and see the individual value at that point. The maximum induced magnetic field is located inside the magnetorquers, with a strength on the order of 10^{-5} Tesla (T). On top of the circuit stack the magnetic field was found to be on the order of 10^{-8} T. According to NOAA software, the magnetic field strength between 200 km and 250 km is between $2.853 \cdot 10^{-5}$T and $2.775 \cdot 10^{-7}$T (NOAA, 2015). The tolerances of the magnetometer require the interference be on the order of 10^{-3} compared to the Earth's magnetic field. This means the interference is right on the cusp of causing measurement errors. If the magnetometer were to

be put in the top U, the field strength would be on the order of 10^{-9}T, and would be negligible compared to the Earth's magnetic field. Given the variability of the strength of the Earth's magnetic field, it is recommended either some form of electromagnetic shielding, or placing the magnetometer in the top U to avoid interference.
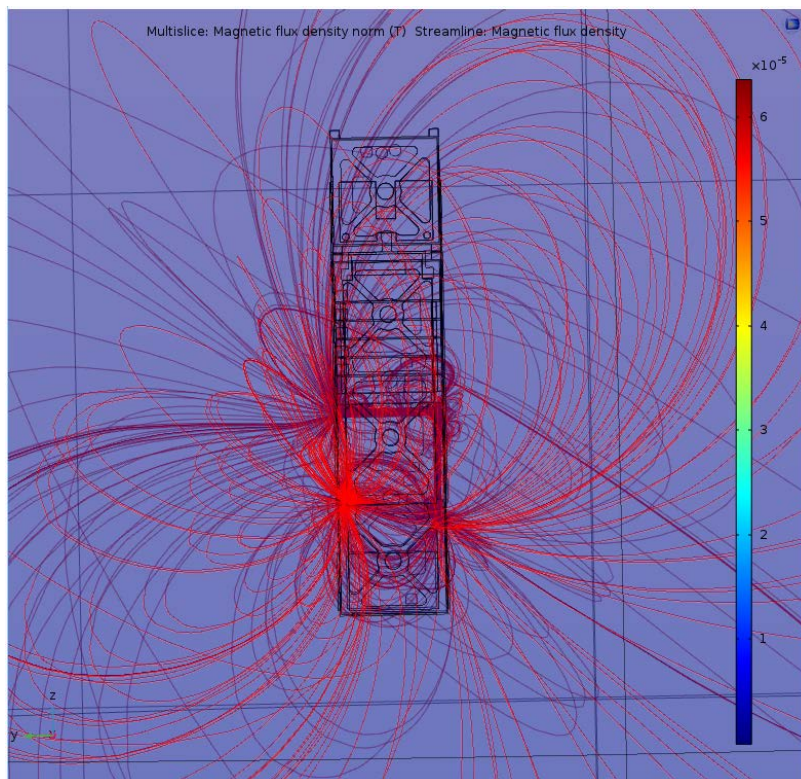
Figure 50: The magnetic field lines from the COMSOL simulation.

5.3 LEO 16U CubeSat Magnetic Field Analysis

5.3.1 Analytical Solution of a Solenoid

In order to perform the magnetic analysis, the magnetorquers were treated as single solenoids. An analytical solution of a single solenoid was obtained to validate the results from COMSOL. The magnetorquer used is the ZARM Technik AG MTO 5.1 used in MQP (MAD-1701). Table 10 shows the parameters used in the calculations that we obtained from MAD-1701. The full data sheet can be found in Appendix B.

Table 10: Analytical Parameters

Variable	Definition	Units	Numerical Value
μ	Magnetic moment	A·m^2	0.5
I	Coil Current	mA	60
A	Coil Area	m^2	1.13 x 10^{-4}
r	Radius of magnetorquer	m	0.006
L	Length of magnetorquer	m	0.09

The first step was to find the number of turns N in the coil from the equation for the magnetic moment μ

$$\mu = NIA \quad \text{Eq. (11)}$$

The 73,746 turns for each magnetorquer. The next step was to solve for the surface current of the coil K_0 using:

$$K_0 = \frac{NI}{L} \quad \text{Eq. (12)}$$

The above equation provides $K_o = 49{,}164$ A/m which was used as an input to COMSOL for the analysis of the magnetorquers.

The analytical value of the magnetic flux density B induced by the magnetorquers given by:

$$B = \frac{\mu K_0}{2} \left\{ \frac{\frac{l}{2r} - \frac{z}{r}}{\sqrt{1 + (\frac{l}{2r} - \frac{z}{r})^2}} + \frac{\frac{l}{2r} + \frac{z}{r}}{\sqrt{1 + (\frac{l}{2r} + \frac{z}{r})^2}} \right\} \qquad \text{Eq. (13)}$$

Where μ is the permittivity of free space which equals $4\pi \cdot 10^{-7}$ H/m. The variable z represents the position along the solenoid where the center is $z = 0$ and the ends are $z = \frac{L}{2}$. Using the above defined and calculated variables, we solved for the magnetic flux density at the center and the ends of the magnetorquer. At $z = 0$, B is approximately 617.78 Gauss while at the ends, B is approximately 308.6 Gauss.

5.3.2 Magnetic Modelling in COMSOL

The magnetic analysis in COMSOL included the main frame, the magnetorquers, and the magnetometer. All other components of the 16U CubeSat were omitted from the magnetic modelling in order to keep the structure as simplified as possible and therefore make the COMSOL analysis run more effectively. A stationary AC/DC model was set up for the analysis using the Electric/Magnetic Fields (No Currents) module, and the structure geometry was imported. The magnetorquers were placed in the 1.5U spaces above where the center thruster unit is placed and oriented along the x, y, and z axes. The magnetometer was placed in the 0.5U space right below the center thruster unit. The main frame was defined as aluminum (7075) while the magnetorquers were defined as copper. For each magnetorquer, the surface current calculated previously was used as an input for the magnetic conservation values. Below in Figure 51, Figure 52 and Figure 53 are the results of the analysis on the 16U. Figure 51 shows the streamlines of the magnetic field. Figure 52 and Figure 53 show the magnetic field strength in the plane of the magnetometer.
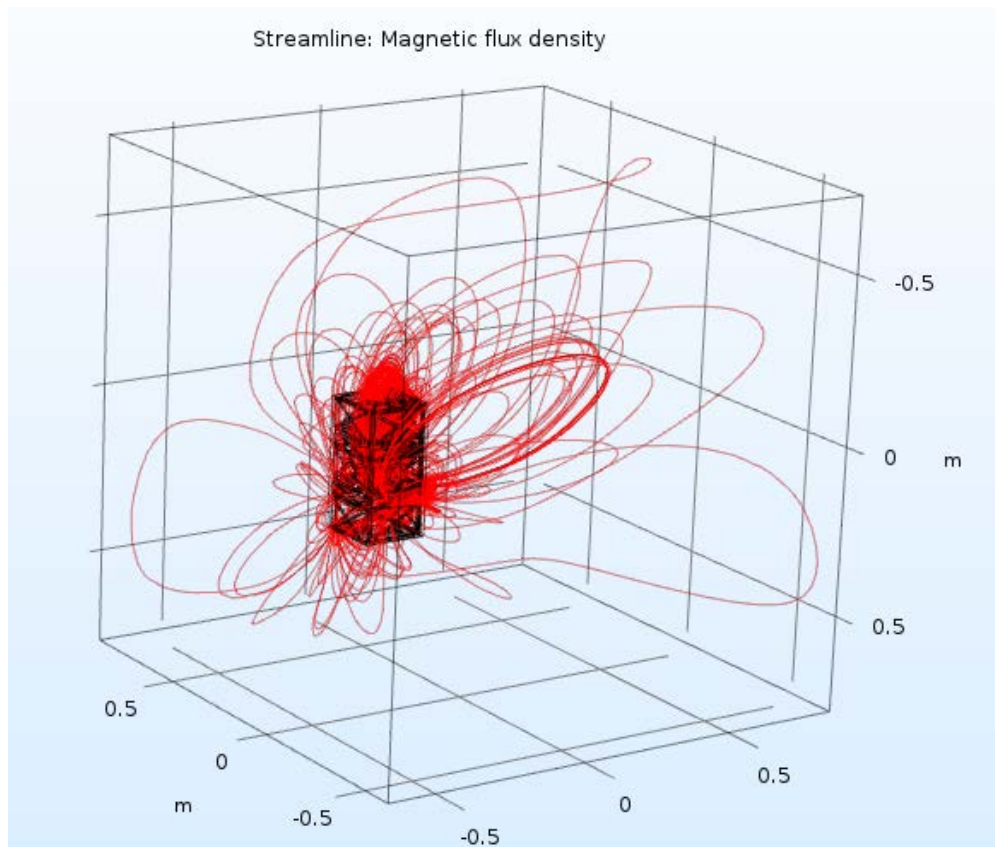
Figure 51: The magnetic field lines from COMSOL simulation.
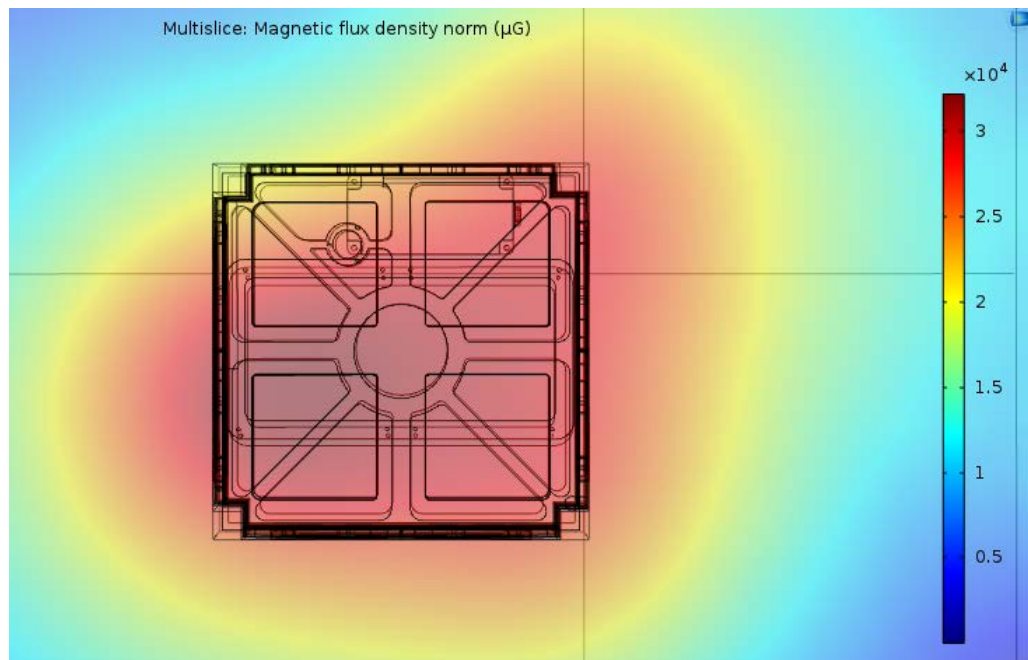
Figure 52: The magnetic flux density from COMSOL simulation.
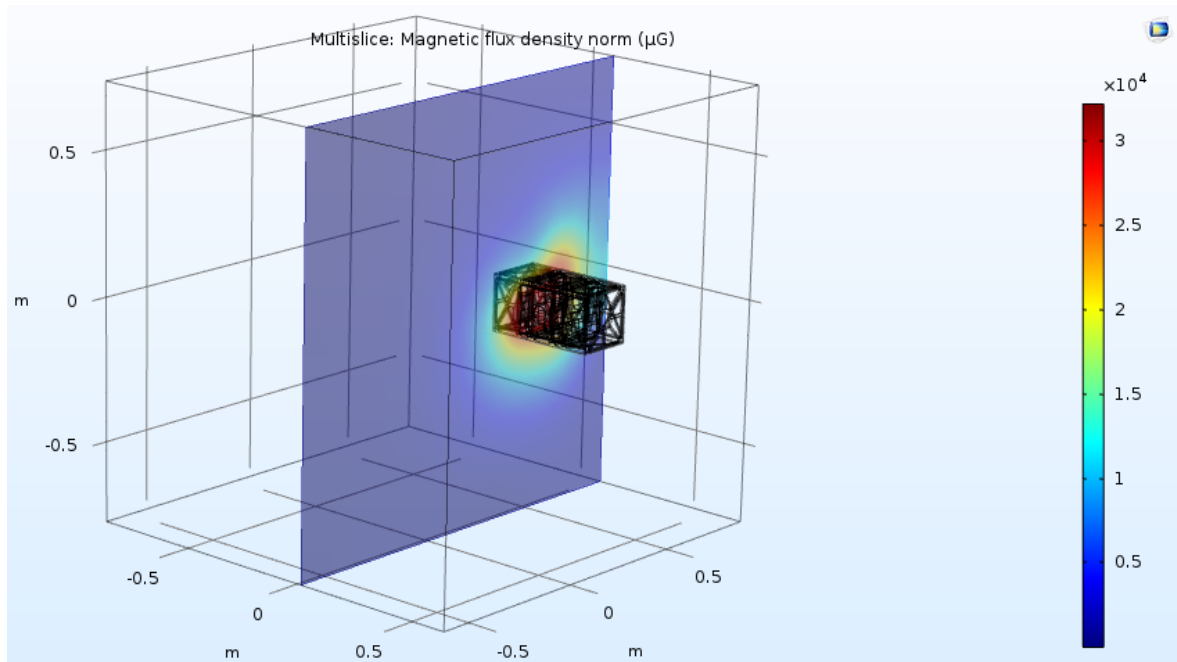
Figure 53: A multislice plot of magnetic flux density from COMSOL simulation.

The results of the analysis are displayed using the streamline and multislice plot options. The streamline plot in Figure 51 shows the magnetic field lines produced by the magnetorquers and where they were the strongest. The maximum field strength calculated is on the order of 0.03 Gauss. This field strength could interfere with magnetometer readings. In order to avoid this problem magnetic shielding should be used to isolate the magnetometer from the magnetic field produced by the magnetorquers.

6 Conclusions and Recommendations

This MQP team was part of a larger effort to design two CubeSats, one for operation in extreme low Earth Orbit, and another to perform orbit raising and rendezvous maneuvers in Low Earth Orbit. There was a total of 16 students assigned in the three teams addressing:

- Mechanical Design, Orbital Analysis, Thermal Analysis and Magnetic Interference Analysis (this project, NAG-1801)

- Power, Telecommunications, Propulsion (JB-1801)

- Structural Analysis, Attitude Determination and Control, Command and Data Handling (MAD-1801)

6.1 eLEO 4U CubeSat

The eLEO mission involves a CubeSat which upon release at about 400 km, lowers its orbit below 250 km and remains at eLEO altitudes for as long as possible using onboard propulsion. The CubeSat carries also pulsed plasma thrusters for attitude control.

6.1.2 Mechanical Design

For the eLEO CubeSat, given the requirements for the mission, it was determined that the solar power which would be provided by a 3U CubeSat would be insufficient to power the required systems during eclipse due to the required locations of the sun sensors. This prompted the design of a 4U structure utilizing a custom produced adapter to attach a 1U frame to a 3U frame. The final 4U design includes all parts, components and subsystems as provided by the two MQP teams (JB1801, MAD 1801).

6.1.3 Orbital Lifetime Analysis

STK was utilized to conduct an orbital lifetime analysis. The eLEO 4U CubeSat is predicted to deorbit 14-24 days after engine shutdown, depending on the final CubeSat mass. This is much shorter than the maximum CubeSat lifespan of 25 years, and the CubeSat is compliant with NASA standards. The body of the CubeSat is likely to completely disintegrate in atmospheric re-entry and will not require a specific deorbiting plan.

6.1.4 Thermal Analysis

The equilibrium temperature of the eLEO CubeSat performed with COMSOL and a de-featured CAD model, ranged on average from around 245 K during eclipse periods and 265 K during illumination periods, but maxed out at 281 K and fell to 236 K near the end of 24 hours in orbit. The maximum temperature reached was the initial temperature of 305 K while the minimum temperature reached was 236 K. The temperatures analyzed over time were documented and observed by creating GIF's, images and videos of the various thermal analysis runs in COMSOL. The simulations show that it is likely the CubeSat will stay inside operational temperature bounds, but some form of thermal regulation may be required to keep the CubeSat inside the operational temperature range if the temperature drops too low. However, the simulations conducted did not include a heat source from the electronics nor the propulsion system, which may alter the results by providing more heat to the system. As such, we recommend additional simulations be conducted which include these sources of heat and a more detailed CAD model, and that some form of passive thermal control be implemented in accordance with the results.

6.1.5 Magnetic Field Analysis

A magnetic interference analysis was conducted using COMSOL. The de-featured CAD model generated for the thermal analysis was augmented with models for 3 magnetorquers, which were

magnetized to $4.7 \cdot 10^{-5}$ T. The simulations showed the interaction between the chassis, circuit stack, and magnetic field lines produced by the firing magnetorquers. It was found that if the magnetometer was placed on top of the circuit stack, the magnetic interference produced by the magnetorquers would be on the order of 10^{-8} T, just large enough to cause small errors in the magnetic field readings. If the magnetometer is put in the top U of the CubeSat, the interference would be on the order of 10^{-9} T, and would not interfere with the readings. Further and more detailed analysis is needed in case magnetorquers are selected for the mission.

It is recommended that the magnetometer be placed in the top U of the CubeSat. Additionally, it is recommended that subsequent teams conduct analysis on the interference that may be produced by firing PPTs.

6.2 LEO 16U CubeSat

The LEO mission involves a CubeSat designed to perform an orbit raising maneuver using onboard propulsion from about 450 km to a higher altitude and subsequently perform a rendezvous or formation flying.

6.2.1 Mechanical Design

The LEO CubeSat underwent many sizing iterations before reaching the final 16U form. The driving design factor was to provide the supporting structure for propulsion and propellant tanks required for these maneuvers. The final design includes all parts, components and subsystems as provided by the two MQP teams (JB1801, MAD 1801). Future design teams considering orbital maneuvers using primary propulsion will probably require sizes 16U to allow for adequate propellant volume. Additionally, future teams should also investigate using deployable solar panels on a non-axis symmetric CubeSat.

6.2.2 Orbital Lifetime Analysis

Using STK the longest anticipated life span of the 16U CubeSat is just over 16 years well below the 25 years required for compliance. Given the size of the CubeSat it is likely to disintegrate upon reentry, thus no specific de-orbit plan was considered.

6.2.3 Thermal Analysis

COMSOL analysis using a de-featured CAD model shows that the components of the 16U CubeSat will remain within operational temperature ranges if exposed surfaces are covered in a material of emissivity 0.55. This material could be a wide range of paints or metallic coatings. With this emissivity only a single component, the GPS, has a risk of reaching a temperature at its operational boundary. The rest of the CubeSat however generally remains within a range of 10-65 degrees Celsius, safe for the majority of commercially available CubeSat components. Passive thermal control measures are sufficient for the CubeSat in any of the three proposed orbits.

6.3.4 Magnetic Field Analysis

If magnetorquers were to be used in place of PPT's onboard the CubeSat, some magnetic shielding may be necessary to use the magnetometer for attitude determination at the same time as using magnetorquers for attitude control. This is due to the magnetorquers producing a field of approximately 0.03 Gauss in the plane of the magnetometer. Alternatively, one could be deactivated while the other is in use. This would slightly delay feedback but increase the accuracy in attitude control maneuvers. Further and more detailed analysis is needed in case magnetorquers are selected for the mission.

It is recommended that the PPT's are used over magnetorquers, to avoid complications in magnetic shielding or having to deactivate attitude determination to use attitude control.

7 References

Agolli, J., Gadoury, J., Rathburn, A., & Demetriou, M. (2017). *Design and analysis of the sphinx-NG CubeSat.* ().

Barnhart, D. J., Vladimirova, T., & Sweeting, M. N. (2007). Very-small-satellite design for distributed space missions. *Journal of Spacecraft and Rockets, 44*(6), 1294-1306. doi:10.2514/1.28678

Bauer, J., Kelley, K., Mello, E., Neu, S., Orphanos, A., Shaffer, T., . . . Blandino, J. (2012). *Mechanical, power, and thermal subsystem design for a CubeSat mission.* ().

Billings, D., Graedel, I., Hoey, F., Lavallee, P., Martinez, N., Torres, J., & Gatsonis, N. (2013). *Design and analysis for a CubeSat mission.* ().

Blandino, J. J., Martinez-Baquero, N., Demetriou, M. A., Gatsonis, N. A., & Paschalidis, N. (2016). Feasibility for orbital life extension of a CubeSat in the lower thermosphere. *Journal of Spacecraft and Rockets, 53*(5), 864-875. doi:10.2514/1.A33462

Blumberg, S. (2017). NASA CubeSat to test miniaturized weather satellite technology. Retrieved from http://www.nasa.gov/feature/goddard/2017/CubeSat-to-test-miniaturized-weather-satellite

Buck, J.CubeSat to demonstrate miniature laser communications in orbit.

Busek Space Propulsion and Systems. (2016). *BET-1mN busek electrospray thurster.* (http://www.busek.com/index_htm_files/70008500%20BET1mN%20Data%20Sheet%20RevH.pdf).

Clyde Space.Custom solutions.

Curci, E., Jacobson, J., Schlack, W., Slabinski, K., & Gatsonis, N. (2017). *Design and analysis for the spinx-NG CubeSat.* ().

Dawson, E., Nassiff, N., Velez, D., & Demetriou, M. (2012). *Attitude determination and control subsystem design for a CubeSat.* ().

Dopart, C., Morlath, R., Oliver, E., Schomaker, J., & Gatsonis, N. (2012). *Design and analysis for a CubeSat mission.* ().

eoPortal directory.CubeSat concept
. Retrieved from https://directory.eoportal.org/web/eoportal/satellite-missions/c-missions/CubeSat-concept#foot1%29

Farhat, A., Ivase, J., Lu, Y., Snapp, A., & Demetriou, M. (2013). *Attitude determination and control system for CubeSat.* ().

Frequently asked questions. (2013). Retrieved
from http://www.CubeSatkit.com/content/faq.html

Gombosi, T. I. (1994). *Gaskinetic theory* (1. publ. ed.). Cambridge u.a: Cambridge Univ. Press.

Hanley, J., Joseph, B., Miller, M., Monte, S., Trudeau, J., Weinrick, R., & Blandino, J. (2013). *Thermal, telecommunication and power systems for a CubeSat.* ().

Heyman Jos. (2009). FOCUS: CubeSats — A costing + pricing challenge.

Howell Elizabeth. CubeSats: Tiny payloads, huge benefits for space research. Retrieved from https://www.space.com/34324-CubeSats.html

ISIS. (2018). CubeSats in brief. Retrieved from https://www.isispace.nl/CubeSats/

J. M. Picone, A. E. Hedin, D. P. Drob, & A. C. Aikin. (2002). NRLMSISE-00 empirical model of the atmosphere: Statistical comparisons and scientific issues. *Journal of Geophysical Research - Space Physics, 107*(A12), 16. doi:10.1029/2002JA009430

Jerry Wright, & Brian Dunbar. (2013). Radiators. Retrieved
from https://www.nasa.gov/mission_pages/station/structure/elements/radiators.html#.VgcSEMtV
hBc

Kewen Zhang, Nikolaos A. Gatsonis, John J. Blandino, & Michael A. Demetriou.Nanosat
orbit raising and rendezvous using a continuous-thrust controller. *55th AIAA aerospace sciences
meeting* () doi:10.2514/6.2017-0163

Ko, D., Ludage, S., Murphy, M., Pelgrift, D., Young, S., & Blandino, J. (2017). *Design and
analysis of the sphinx-NG CubeSat.* ().

Kramer, H. (2018). CubeSat concept. Retrieved
from https://directory.eoportal.org/web/eoportal/satellite-missions/c-missions/CubeSat-concept

Mabrouk Elizabeth. What are SmallSats and CubeSats? Retrieved
from https://www.nasa.gov/content/what-are-smallsats-and-CubeSats

Michael. (2009). Michael's list of CubeSat satellite missions. Retrieved
from http://mtech.dk/thomsen/space/CubeSat.php

Mikron. *Table of emissivity of various surfaces.* ().Mikron Instrument Company.

Mr. Hank Heidt , Prof. Jordi Puig-Suari , Prof. Augustus S. Moore , Prof. Shinichi Nakasuka ,
Prof. Robert J. Twiggs.CubeSat: A new generation of picosatellite for education and industry
low-cost space
experimentation. Retrieved
from https://digitalcommons.usu.edu/cgi/viewcontent.cgi?referer=https://www.google.com/&htt
psredir=1&article=2069&context=smallsat

NAG 1204 design and analysis for a CubeSat mission

NASA. (2015). *MSIS-E-90 atmosphere model*. Online:

NASA. (2018). CubeSats overview. Retrieved

from https://www.nasa.gov/mission_pages/CubeSats/overview

NASA JPL. (2017). Magnetometer (MAG). Retrieved

from https://saturn.jpl.nasa.gov/magnetometer/

Nikolaos A. Gatsonis, Ye Lu, John J. Blandino, Michael A. Demetriou, & Nicholas

Paschalidis.Micro pulsed plasma thrusters for attitude control of a low earth orbiting

CubeSat. *54th AIAA aerospace sciences meeting* () doi:10.2514/6.2016-0692

NOAA. (2015). *The world magnetic model and associated software*. online:

Paine, T.*AMES cost model.* ().NASA.

Sivaprakash, N., & Shanmugam, J. (2005). Neural network based three axis satellite attitude

control using only magnetic torquers. Paper presented*, 2* 6 pp. Vol. 2.

doi:10.1109/DASC.2005.1563440

Screencast-O-Matic (Version 2.1.8) [Computer software]. (n.d.). Retrieved March 2, 2018,

from https://screencast-o-matic.com/

Space GPS receiver.

The Aerospace Corporation. (2018). Spacecraft reentry. Retrieved

from http://www.aerospace.org/cords/all-about-debris-and-reentry/spacecraft-reentry/

Thermacoax.Electrical heating system on spacecraft. Retrieved from http://www.thermocoax-

space.com/electrical-heating-system/

Waydo, S., Henry, D., & Campbell, M. (2002). CubeSat design for LEO-based earth science

missions. Paper presented at the *, 1* 1. doi:10.1109/AERO.2002.1036863

Zhu, L., Raman, A., Wang, K. X., Anoma, M. A., & Fan, S. (2014). Radiative cooling of solar

cells. *Optica, 1*(1), 32. doi:10.1364/OPTICA.1.000032

8 Appendices

Appendix A

Heat flux calculation MATLAB file

```
%% heat flux%%

%%Patrick Kroyak 2018%%


alpha = .9; %.89~.92 for spacecraft usually

gamma =1.4;

u = 7600; %spacecraft speed

n_i= 3.127*10^-13; %particle density, found usis msis

Ti = 2000; %%%% atmosphere temp

k = 1.38*10^-23; %boltzmann

P_i = n_i*k*Ti; %incident pressure, boltzmann distribution

r= 2; %approximation for a very fast s/c

st = .25;  %approximation for a very fast s/c

Tw = 100; %% spacecraft

R = 8.314; %j/kgmol

a = sqrt(gamma*R*Ti); %speed of sound

M = u/a; %%mach number

s = u*sqrt(M/(2*k*Ti)); %% s factor

gammaratio=(gamma+1)/(gamma-1); %%% less messy using this in final formula


flux=alpha*gammaratio*P_i*u*(1+((gamma-1)/(gamma+1))*(s^2)*r-(Tw/Ti))*st
```
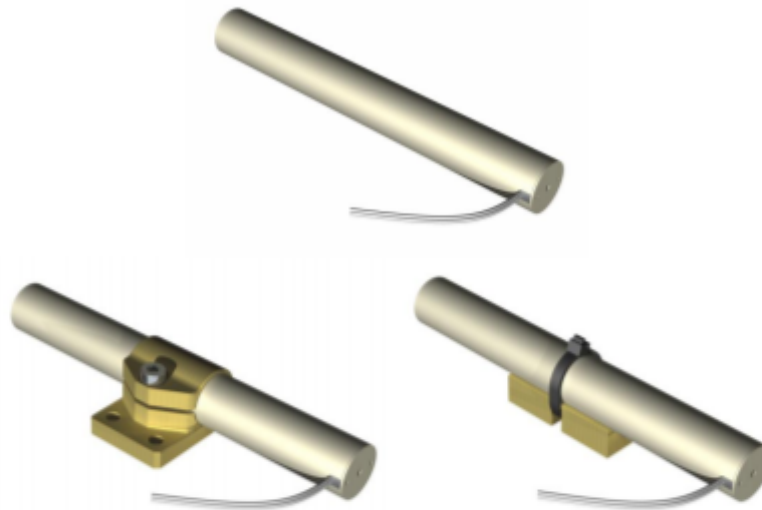
Appendix B (MAD-1701)

	ZARM Technik AG **Magnetic Torquers**	Doc. No.: MT0.5-ZAR-MTR-01 Issue: 2 Date: 20.09.2016 Page: 1 of 1

MT0.5-1 Technical Performance Data Sheet

Performance Data	MT0.5-1-01	Tolerance, remark
Maximum linear dipole range	> ± 0.5 Am^2	at max. linear current
Linear dipole current range	± 60 mA	at maximum linear dipole moment
Linear dipole power consumption	0.3 W	± 5 % (20.0 °C)
Linear dipole supply voltage range	± 5 V DC	± 5 % (20.0 °C)
Linearity error	< 1 %	within linear dipole moment range
Residual dipole	< 0.5 %	of maximum linear dipole moment
Coil resistance	83 Ω	± 5 % (20.0 °C)
Magnetic dipole step response time constant τ (63% value)	10 ms	± 20 % (20.0 °C)
Connector	Flying Leads	
Overall unit mass	0.05 kg	± 5%
Unit Length	≤ 94 mm	overall unit length
Unit Height / Width	16 mm / 33 mm	with heritage bracket
Unit Height / Width	20 mm / 12 mm	with V-bracket

Appendix C

Table 11: The material properties for thermal analysis of eLEO CubeSat.

Material	Density (kg/m³)	Thermal Conductivity (W/m-K)	Heat Capacity (J/kg-K)
Aluminum 5052-H32	2680*	138*	900*
*Material Properties retrieved from (Ko et al., 2017).			

Appendix D

Table 12: Illumination and eclipse orbit time for the eLEO CubeSat after 4 hours.

Time (seconds)	Time sum (min)	Illumination or Eclipse
0 - 507	8.45	illumination
508 - 2703	36.58333	eclipse
2704 - 5848	52.4	illumination
5849 - 8043	36.56667	eclipse
8044 - 11189	52.41667	illumination
11190 - 13384	36.56667	eclipse
13385 - 14400	16.91667	illumination

Appendix E: De-featured model creation

This Appendix details the assembly of the simplified model for thermal analysis. This model was created to remain true to the geometry of the CubeSat, and positioning of each component within it, while simplifying the geometries of individual parts to allow for simulation. The imported model was covered in a frame that would block the PPT's from firing, this was to ensure that appropriate surface area was represented in the model. The baseline thermal model and the GPS location are shown in Figure 54 and Figure 55.

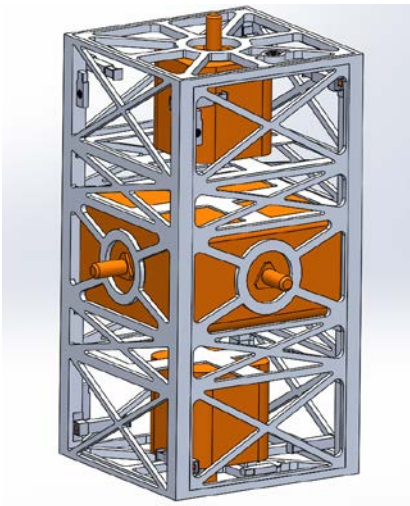The frame, thrusters, PPT's, and sun sensors remain the same.
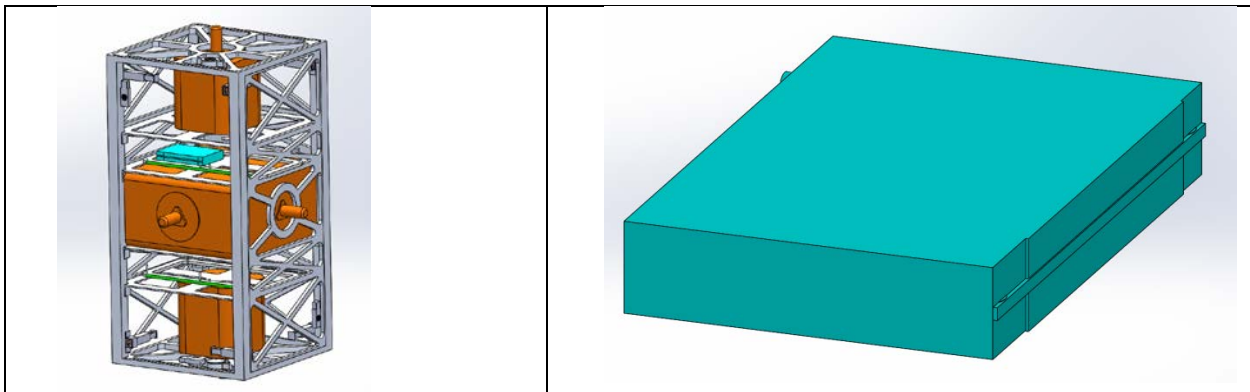

Figure 54: The baseline thermal model of the 16U.

Figure 55: The GPS model and location for the 16U.

Appendix F: Circuit Stack Models and Positions

The circuit stack was replaced by a cube of the dimensions of the stack, which is shown in Figure 56. This is the largest simplification in the thermal analysis but is necessary to model the heat transfer to the component.
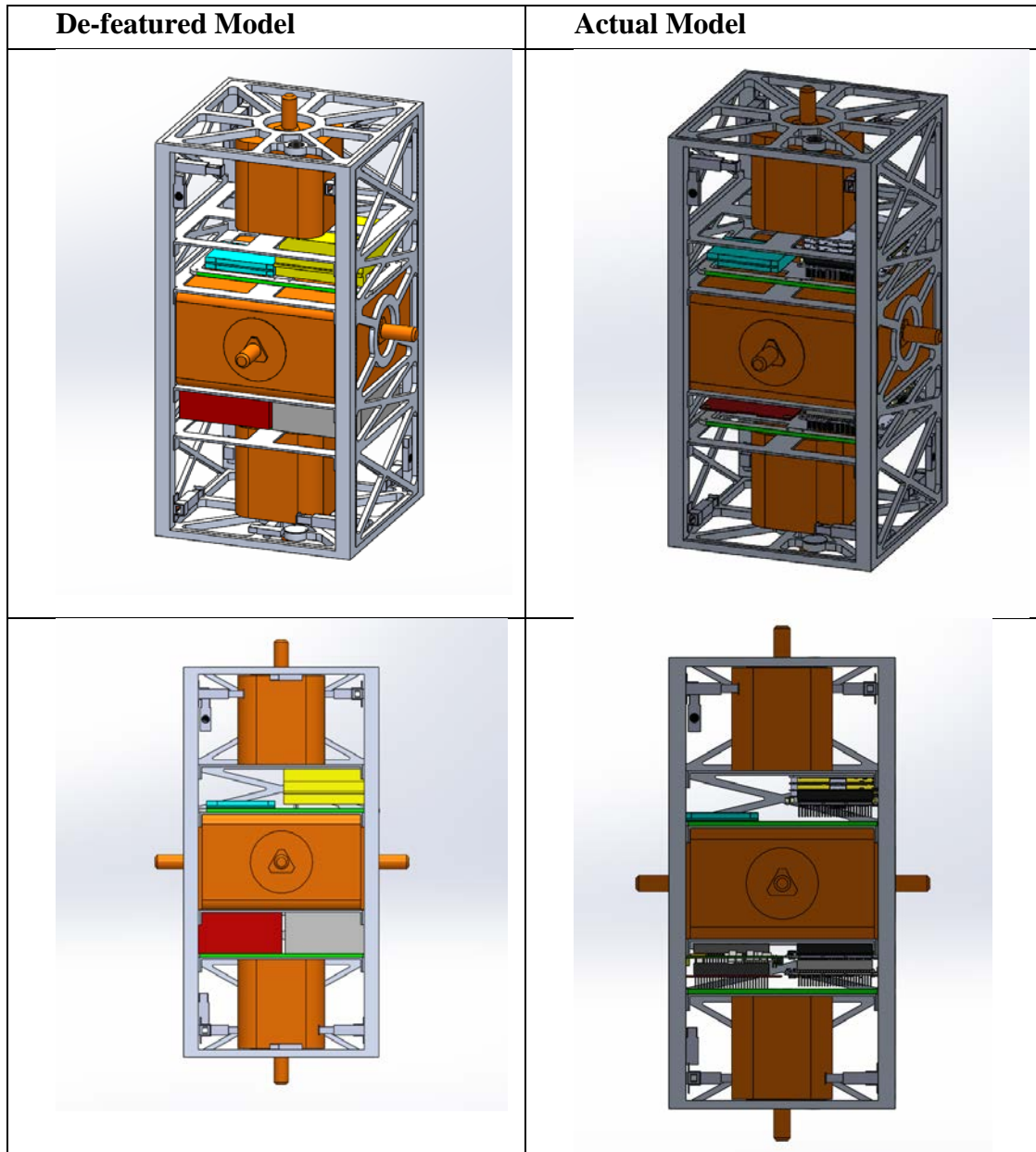
De-featured Model	Actual Model

Figure 56: The circuit stack model and position vs the actual circuit stack position.

Appendix G: Magnetometer

Figure 57 shows the location and geometry of the magnetometer for the simplified and actual models.
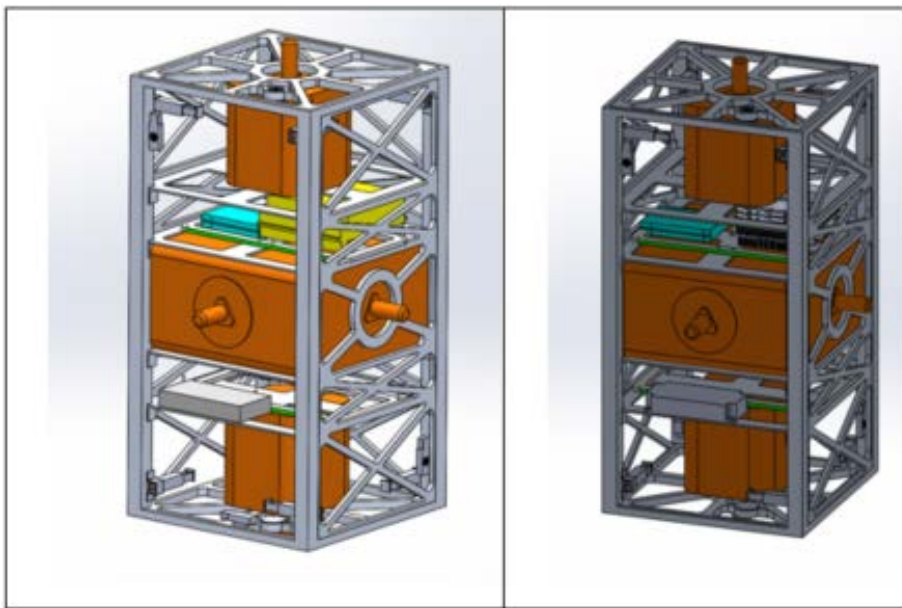

Figure 57: The magnetometer model used vs the actual model and position.

Appendix H: Solar Panels and Antenna

Figure 58 shows the solar panels and antenna on the simplified model.
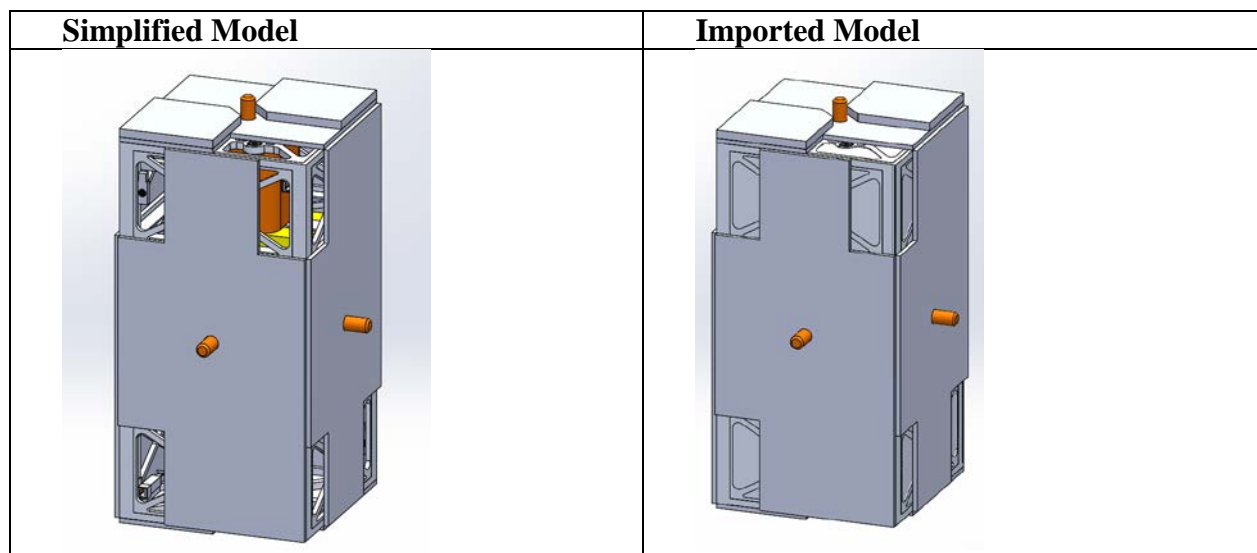
Simplified Model	Imported Model

Figure 58: The solar panels and antenna shown in position on the 16U model.